A. 1-68-89-I
July 20, 1968

TM-151
2610.1
2630.1

FAKE STUDIES OF SOME STRONG AND WEAK INTERACTIONS IN THE 12-FT AND 25-FT BUBBLE CHAMBERS

PART I. NEUTRINO INTERACTIONS

M. Derrick
Argonne National Laboratory

T. O'Halloran
University of Illinois

and

R. Kraemer
Carnegie-Mellon University

Introduction

To help clarify the problem of the parameters of the proposed 25-ft chamber and to provide a basis of comparison between the ANL 12-ft chamber and the proposed 25 ft, we have generated a number of reactions using the program FAKE. Studies of this kind have previously been made by Chinowsky[1] for ν-induced reactions and by Plano[2] for pion interactions. The present work differs from that previously carried out in that more realistic parameters are used for the chambers and a greater range of event types and energies have been generated.

Error Formulae and Chamber Parameters

We do not discuss the derivation of the error formulae used, since the form of the equations is relatively well known, but merely write down the expressions and constants.[3]

Coulomb term

$$\frac{\Delta p}{p} = \frac{1.5}{\cos\lambda\, \ell^{1/2} H\beta}$$

$$\Delta\phi = \frac{0.23\, \ell^{1/2}}{p\beta \cos\lambda}$$

$$\Delta\lambda = \frac{0.23\, \ell^{1/2}}{p\beta}$$

Measuring term

$$\frac{\Delta p}{p} = \frac{1.9\times10^{-3}\, p\epsilon}{\ell^2 H \cos\lambda}$$

$$\Delta\phi = \frac{3.8 \times 10^{-4}\, \epsilon}{\cos\lambda}$$

$$\Delta\lambda = \frac{3.0 \times 10^{-4}\, \epsilon \cos\lambda}{\ell} \sqrt{1 + \frac{\tan^2\lambda}{9}}$$

Floors were put on λ and ϕ of values:

12-ft chamber		25-ft chamber	
$\Delta\phi$	$\Delta\lambda$	$\Delta\phi$	$\Delta\lambda$
0.9×10^{-4} rads	1.5×10^{-4} rads	0.7×10^{-4} rads	1.1×10^{-4} rads

where:

ℓ = track length in cms

H = magnetic field in kG

p = momentum in MeV/c

ϵ = setting error in space in microns

ϕ = azimuthal angle

λ = dip angle

β = v/c.

Chamber Parameters

The 12-ft chamber was taken to be a cylinder of radius 2 m and depth 2 m, which is approximately the dimensions of the real ANL chamber. For the 25-ft we scaled things to a radius of 4 m and depth of 3 m. This was done for convenience and not because we felt that a pillbox-shaped

chamber is best. The difference between this and the football shape proposed by BNL should not be of any consequence.

The setting error in space (ϵ) for the 12-ft chamber is taken as 250μ. The appendix[4] to the report written by M. Derrick and R. Kraemer lists the different contributions to the point-reconstruction accuracy for the 12-ft chamber. The error is dominated by thermal turbulence of the liquid hydrogen which multiple scatters the rays of light travelling from the bubble to the camera lens. This effect varies as the distance to the 3/2 power as is characteristic of a multiple scattering. It also varies almost linearly with the heat flux through the visible volume of the chamber.[4] Assuming the same heat flux, then the setting accuracy in the 25 ft will be two to three times worse than in the 12 ft since the 25-ft chamber as presently proposed[5] is about twice as deep as the 12 ft. It is also an empirical fact that with chambers presently in use the setting error scales with the chamber size although there are significant variations between chambers of roughly the same size but of different designs. We, therefore, use 250μ for the 12-ft chamber and 500μ for the 25 ft as best guess setting errors. The other two cases we consider are a magnetic field of 40 kG on the 12-ft chamber and an optimistic setting error of 250μ for the 25-ft chamber, giving a total of four different parameter sets listed later.

Neutrino Interactions Generated

We consider the problem of separating the elastic neutrino events:

$$\nu + n \rightarrow \mu^- + p, \qquad (1)$$

from the same reaction with an additional π^o. Since the inelastic channel is dominated by $N^*(1238)$ production, we generated the reaction

$$\nu + n \rightarrow \mu^- + N^{*+} \hookrightarrow p + \pi^o. \qquad (2)$$

The resulting final state $\mu^- p \pi^o$ is not over-constrained since the ν momentum is not known for any individual event, so one can only obtain a 0c solution. The events were generated with a peripheral angular distribution similar to that expected from the known form factors. The distribution actually used was $d\sigma/dt \propto e^{4t}$, with t in $(GeV/c)^2$. The beam was spread out over the whole width of the 12-ft chamber but restricted in depth to the center of the chamber. Some events should perhaps be generated at other depths. For the 25-ft chamber the beam width was not changed, so only the central 4 m were illuminated by the ν beam.

ν Spectrum

Two ν spectra were used. First, a white spectrum typical of a wide-band beam was generated. Figure 1 shows the ν spectrum represented by the 500 events used in this part of the study. It peaks at about 4 GeV and goes up to 20 GeV. Second, a typical narrow-band spectrum peaking at 10 GeV was used, as shown in Fig. 3.

A total of 16 different sets of data, each consisting of 500 events, were generated with the following chamber parameters:

	Chamber	Field	Setting Error
1	12 ft	20 kG	250μ
2	12 ft	40 kG	250μ
3	25 ft	40 kG	250μ
4	25 ft	40 kG	500μ

and the two spectra:

1) white and 2) monochromatic,

and the two event types:

1) elastic reaction (1) and 2) inelastic reaction (2).

Results of FAKE

Figures 2 and 3 show the muon spectra resulting from the two ν spectra for the elastic events. It is clear that the muon spectrum follows the ν spectrum quite closely, which comes from the fact that the reactions are peripheral. Figure 4 shows the proton momentum spectrum from the elastic events. The proton spectra do not depend strongly on the ν spectrum but only on the reaction type and momentum transfer dependence. For the elastic events most protons are below 1 GeV/c and, so, will come to rest in the bubble chamber. With deuterium in the chamber a large fraction of the protons will interact before stopping or leaving the chamber, but this is not of major importance since the momentum is low and well measured with only a small length of proton track.

The angular distribution of the protons is quite different for the N^* and elastic events as seen in Fig. 5. The elastic protons tend to come

out near 90° to the beam direction, although the $\mu^- \nu$ mass difference restricts the maximum proton angle slightly, whereas the protons from the N^* decay have a quite different angular distribution.

These factors all enter into the transverse momentum unbalance shown in Figs. 6 and 7. The measurement accuracy is such that even for the 12-ft chamber with 20 kG and a 10-GeV ν beam the transverse momentum balance is good to approximately 15 MeV/c for the elastic events, whereas for the N^* production a more typical value is 200 MeV/c which represents mainly the transverse momentum of the π^o.

Two important effects are not included in the P_T unbalances shown in Fig. 6. The first is the Fermi motion in the deuteron. In small chambers one can measure a spectator proton if its momentum is less than 80-100 MeV/c. The new chambers will probably be worse than this because of the relatively poor space resolution. Since the spectators are isotropic, the invisible spectator events will give an average P_T uncertainty of approximately 40 MeV/c. The uncertainty in the direction of the ν which is typically a few mrads will add a comparable uncertainty; i.e., $P_\nu \cdot \theta_\nu \sim 10 \text{ GeV} \cdot 3 \cdot 10^{-3}$ or 30 MeV/c for the monochromatic beam. The conclusion is that measuring error in the bubble chamber is not very important for this class of event, so one can use the full length of both the 12-ft and 25-ft chambers for the interaction volume.

Results of Kinematic Fitting

About 100 events in each of the 16 cases have been fit using GRIND.

In generating the events the ν-beam direction was fixed and only the momentum was varied for each event according to the spectra shown in Figs. 1 and 3. Both the momentum and angles of the secondary tracks were smeared within the errors. In fitting the events for the white spectrum the momentum was considered unmeasured, whereas the azimuth and dip-angle errors were fixed at 5 mrad.

The elastic events always gave a satisfactory 3c fit for all chamber and beam combinations. The probability distribution was not uniform, but biassed towards higher probabilities because of the beam angle errors. The fitted values did not vary significantly between the worst (12 ft, 20 kG, 250μ) and the best (25 ft, 40 kG, 250μ) conditions. Table I gives the parameters for a typical event.

For the white spectrum no event generated as $\mu^- N^{*+} \rightarrow \mu^- p \pi^o$ gave a fit to the elastic hypothesis $\mu^- p$ even in the 12-ft chamber with 20 kG. With the monochromatic spectrum, which is essentially a 10-GeV ν beam, two N^* events with very short muon tracks 0.9 cm and 15.1 cms respectively gave fits to the elastic hypothesis but neither would fit the remaining three chamber parameter sets since for those cases the muon momentum was better determined.

An important conclusion from these studies is that the tighter ν momentum provided by the narrow-band beam is not needed for the kinematics. The narrow-band beam then only reduces the overall ν flux and with it the background in the chamber.

Many of the elastic events also gave a 0c solution with an additional

π^o. For both ν spectra and for all chamber parameters almost exactly one-half of the elastic events gave such a 0c solution. The events are easy to separate from the events with a real π^o production, since the pseudo π^o's all go in the direction of the ν beam, as is intuitively obvious, whereas the π^o distribution from the N^* events is approximately isotropic. It is clear that for the events considered here the 0c solution for the elastic events is no problem.

In general this ambiguity will always exist, and, so if there is a class of events which give a π^o in the forward direction, downstream γ-conversion plates would be needed to sign the real events. The design of the 25-ft chamber should take that into account.

Figure 8 shows the end points of the tracks (including the ν interaction point) for the white spectrum in the 25-ft chamber. Most of the muons are swept out of the side of the chamber. If one plans to use spark chambers to label the tracks as hadron or lepton, then access to the chamber will be needed at the side as well as the end.

Conclusion and Possible Further Studies

This report covers the most copious kind of event which bears on the form factor question and concludes that both the 12-ft and 25-ft chambers have plenty of precision. One could extend the immediate study to higher energies, but things will probably vary rather slowly, since the momentum transfer distribution is expected to depend only weakly on the ν energy and in this work is considered to be independent of energy.

When real data of the interactions of ν and $\bar{\nu}$ on free nucleons are available from ANL and BNL, one can use this data to extrapolate to NAL and the 25-ft chamber to make a more realistic simulation.

The problems seem to be more in the beam and backgrounds in the chamber rather than in the basic precision of the device, which is clearly more than adequate.

REFERENCES

[1] W. Chinowsky, 200-BeV Accelerator: Studies in Experimental Use, Lawrence Radiation Laboratory UCRL-16830, Vol. II, 1965, p. 53.

[2] R. J. Plano, op. cit., Vol. III, 1966, p. 256.

[3] R. L. Gluckstern, Nucl. Instr. and Methods, 24, 321 (1963).

[4] L. R. Turner, Limits of Track Location Determination in the 12-ft HBC, ANL-BBC-110 (unpublished).

[5] 25-Ft Cryogenic Bubble-Chamber Proposal, Brookhaven National Laboratory BNL-12400, 1968.

Table I. Elastic Neutrino Event in 12-Ft and 25-Ft Chambers.

Masses in GeV, Momenta in GeV/c, Angles in radians, Lengths in cms

12-ft Chamber 20 kG 250μ

FITBANKS		TRK	P	DIP	PHI	DP	DDIP	DPHI	L	DL
1	0.1057	1	9.1293	0.0503	0.0133	0.0554	0.0005	0.0008	241.59	0.06
2	0.9383	2	0.4953	-1.2130	5.5620	0.0188	0.0120	0.0478	74.85	0.20

FIT NOPT 1 NOTR 3 TYP 1010 HYP 1 ER14 NONE ER15 NONE CHISQ 1.33 ND 3 PROB 0.7228 STEP 2

						Unfitted Values and Errors						Fitted Values and Errors					
TRACK	MASS	CODE	BUB	ION	P	DIP	PHI	DP	DDIP	DPHI	P	DIP	PHI	DP	DDIP	DPHI
A0 0	0.0000	UWWF	10	K	9.245	0.000	3.142	0.000	0.005	0.005	9.231	-0.000	3.142	0.052	0.000	0.000
A3 +	0.9383	WWWF	99	K	0.485	-1.213	5.562	0.004	0.012	0.048	0.487	-1.207	5.563	0.004	0.008	0.023
A2 -	0.1057	WWWF	10	K	9.129	0.050	0.013	0.055	0.001	0.001	9.113	0.050	0.013	0.052	0.000	0.001

25-ft Chamber 40 kG 250μ

FITBANKS		TRK	P	DIP	PHI	DP	DDIP	DPHI	L	DL
1	0.1057	1	9.0997	0.0506	0.0125	0.0139	0.0007	0.0009	618.62	0.06
2	0.9383	2	0.4907	-1.2130	5.5620	0.0113	0.0124	0.0493	74.85	0.20

FIT NOPT 1 NOTR 3 TYP 1010 HYP 1 ER14 NONE ER15 NONE CHISQ 0.57 ND 3 PROB 0.9042 STEP 2

						Unfitted Values and Errors						Fitted Values and Errors					
TRACK	MASS	CODE	BUB	ION	P	DIP	PHI	DP	DDIP	DPHI	P	DIP	PHI	DP	DDIP	DPHI
A0 0	0.0000	UWWF	10	K	9.215	0.000	3.142	0.000	0.005	0.005	9.217	-0.000	3.142	0.014	0.000	0.000
A3 +	0.9383	WWWF	99	K	0.485	-1.213	5.562	0.004	0.012	0.049	0.486	-1.211	5.574	0.004	0.008	0.025
A2 -	0.1057	WWWF	10	K	9.100	0.051	0.012	0.014	0.001	0.001	9.099	0.050	0.012	0.014	0.000	0.001

TM-151
2610.1
2630.1

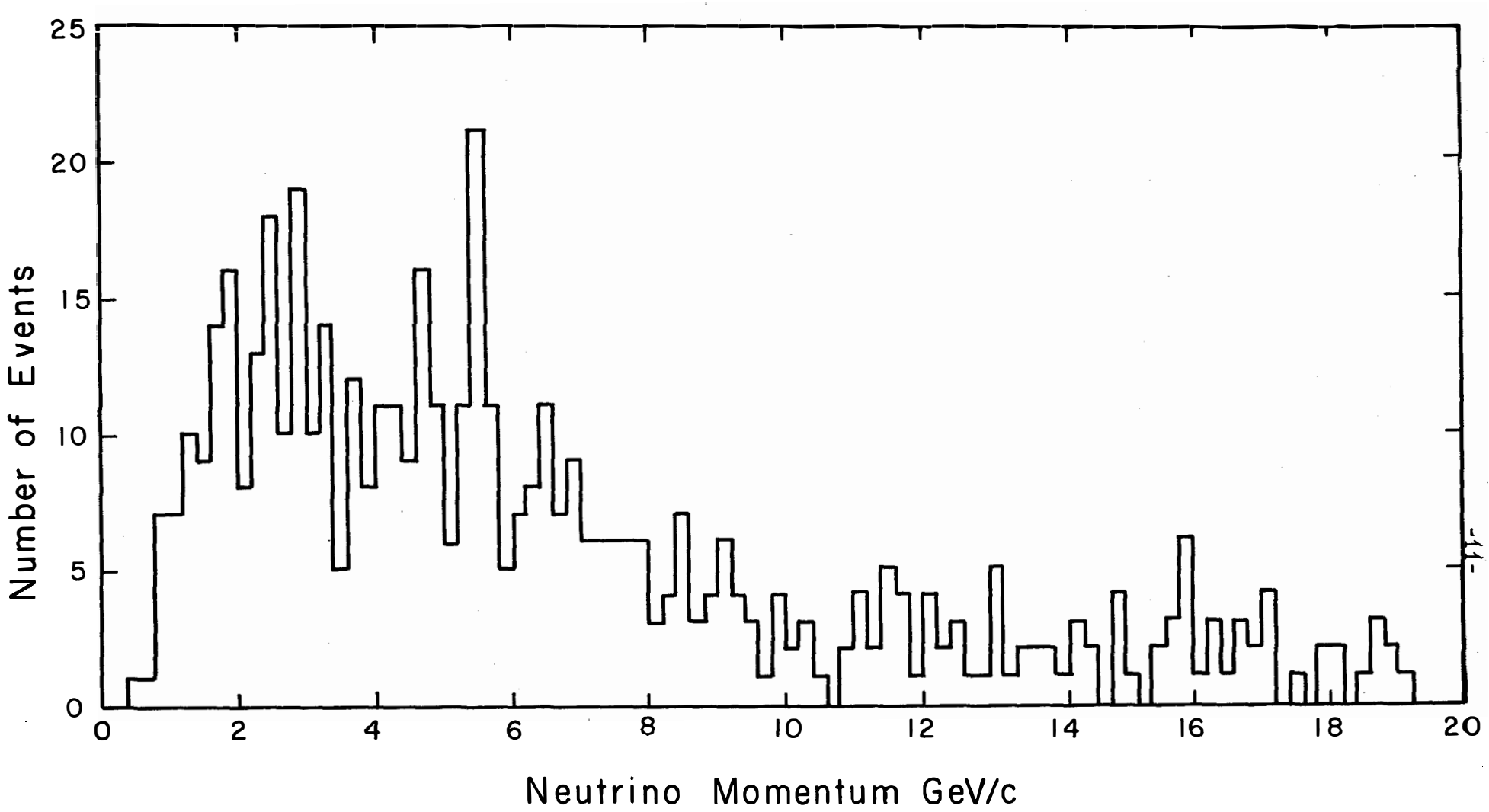

Fig. 1. White neutrino momentum spectrum.

TM-151
2610.1
2630.1

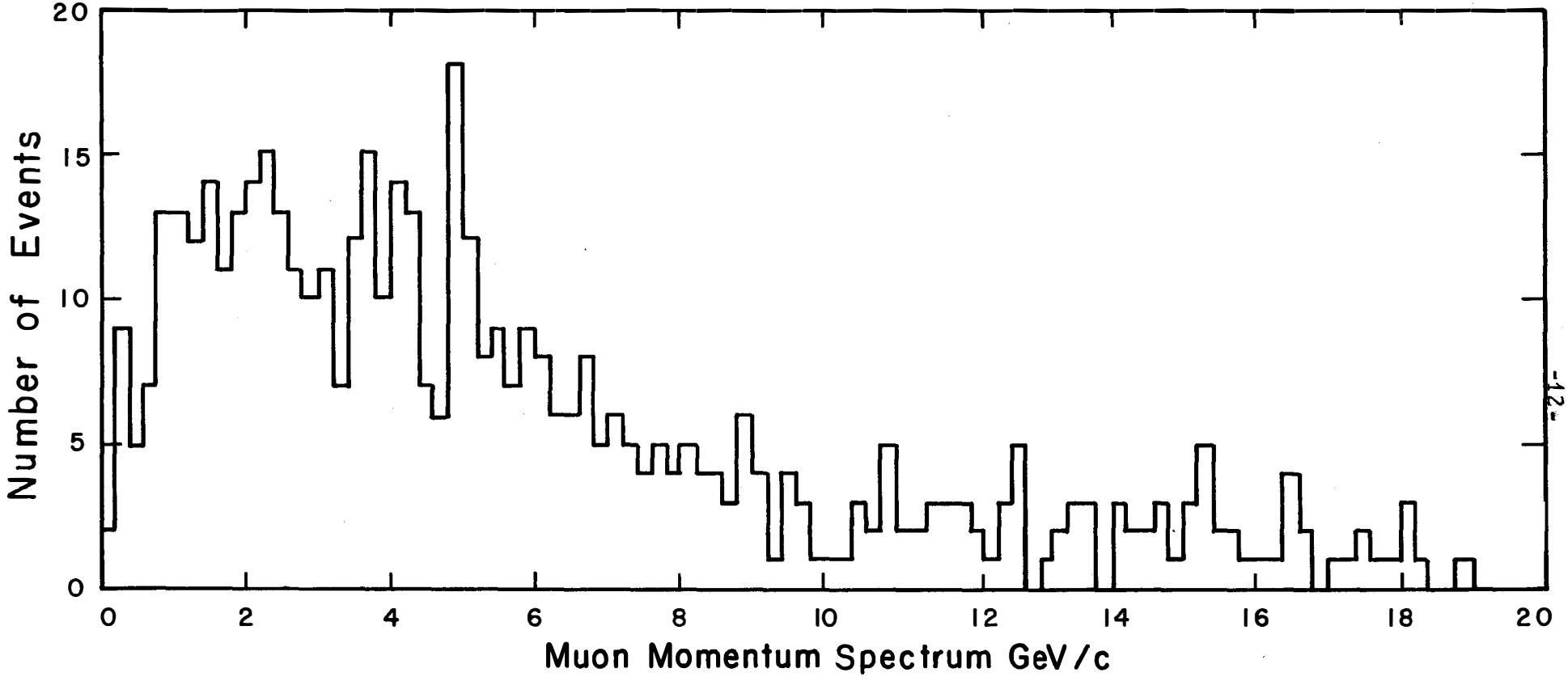

Fig. 2. Muon momentum spectrum from elastic event $\nu + n \rightarrow \mu^- + p$, using white neutrino spectrum.

TM-151
2610.1
2630.1

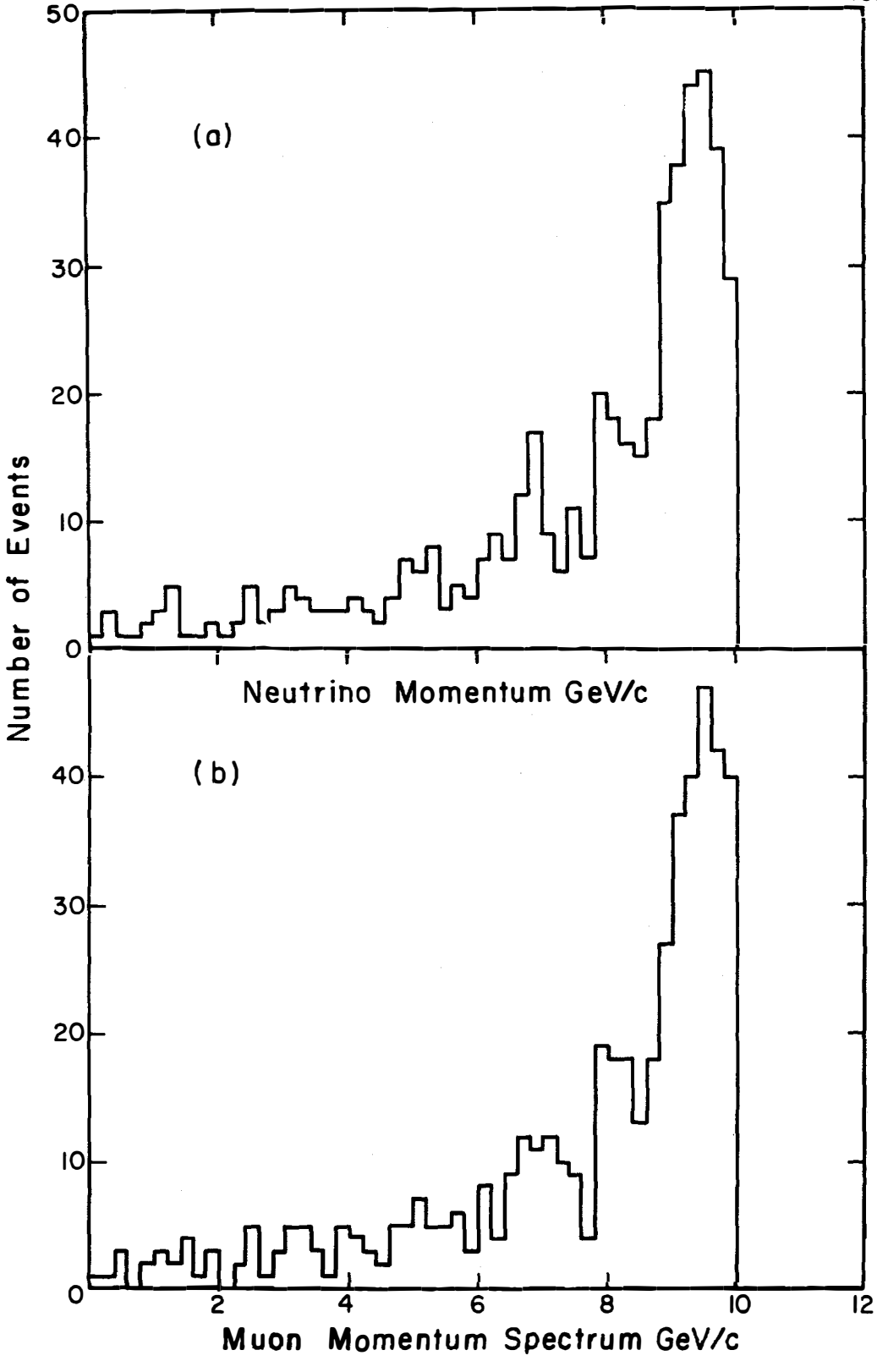

Fig. 3(b). Muon spectrum resulting from elastic scattering of the narrow-band neutrino spectrum of Fig. 3(a).

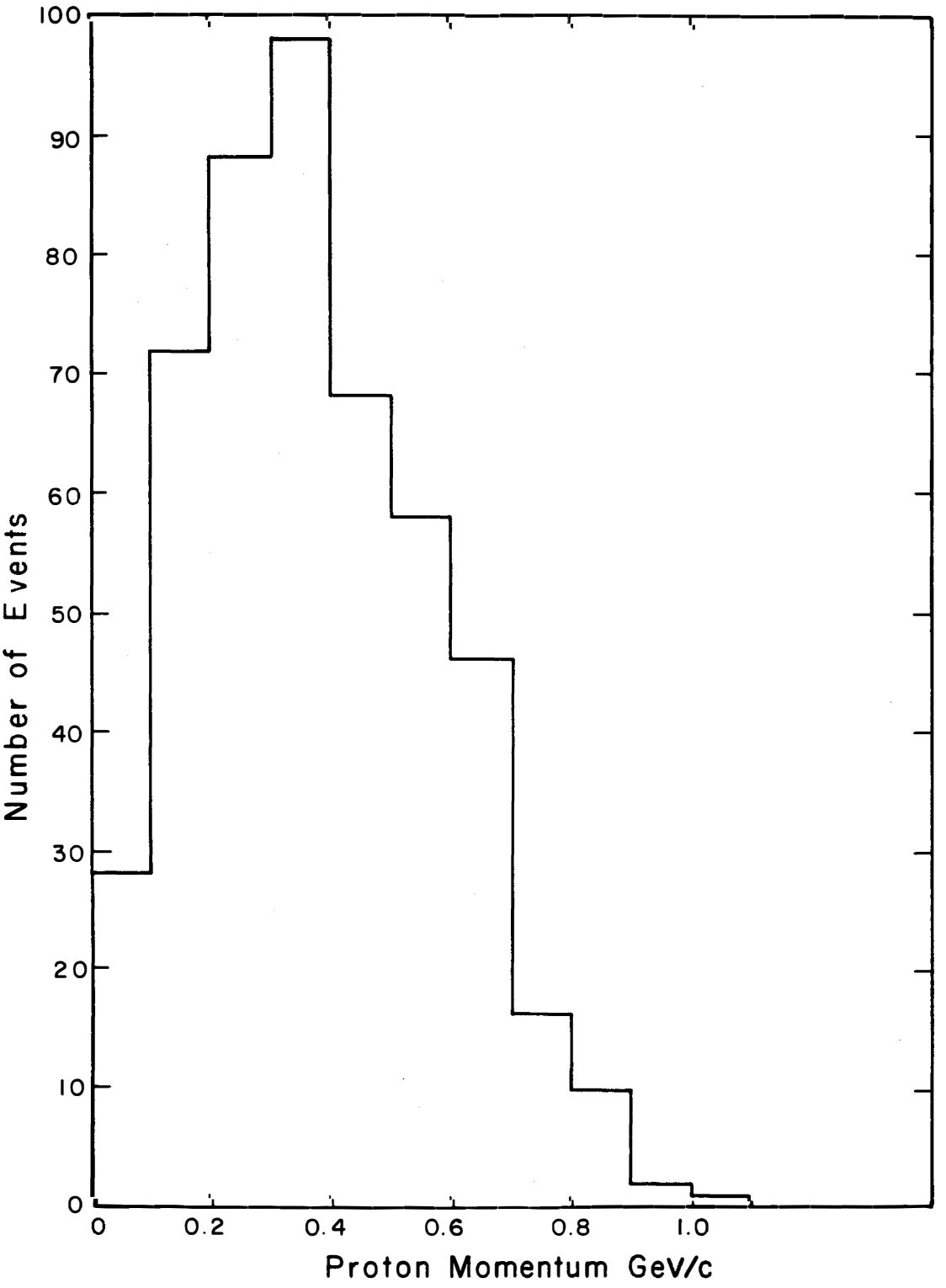

Fig. 4. Elastic proton spectrum from $\nu + n \rightarrow \mu^- + p$ with narrow-band neutrino spectrum of Fig. 3(b).

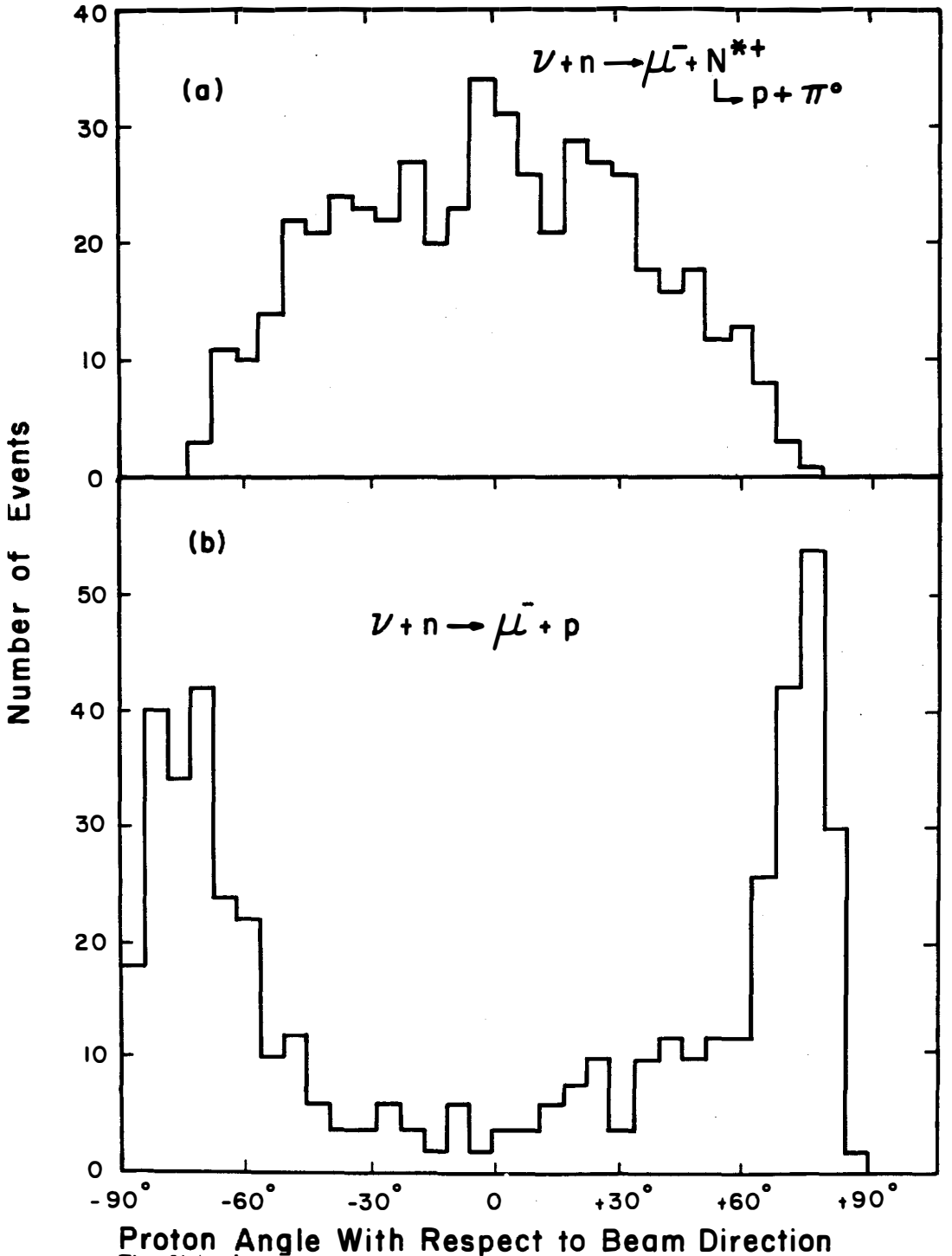

Fig. 5(a). Angular distribution of protons from isobar decay in inelastic reactions; (b) Angular distribution of elastic protons.

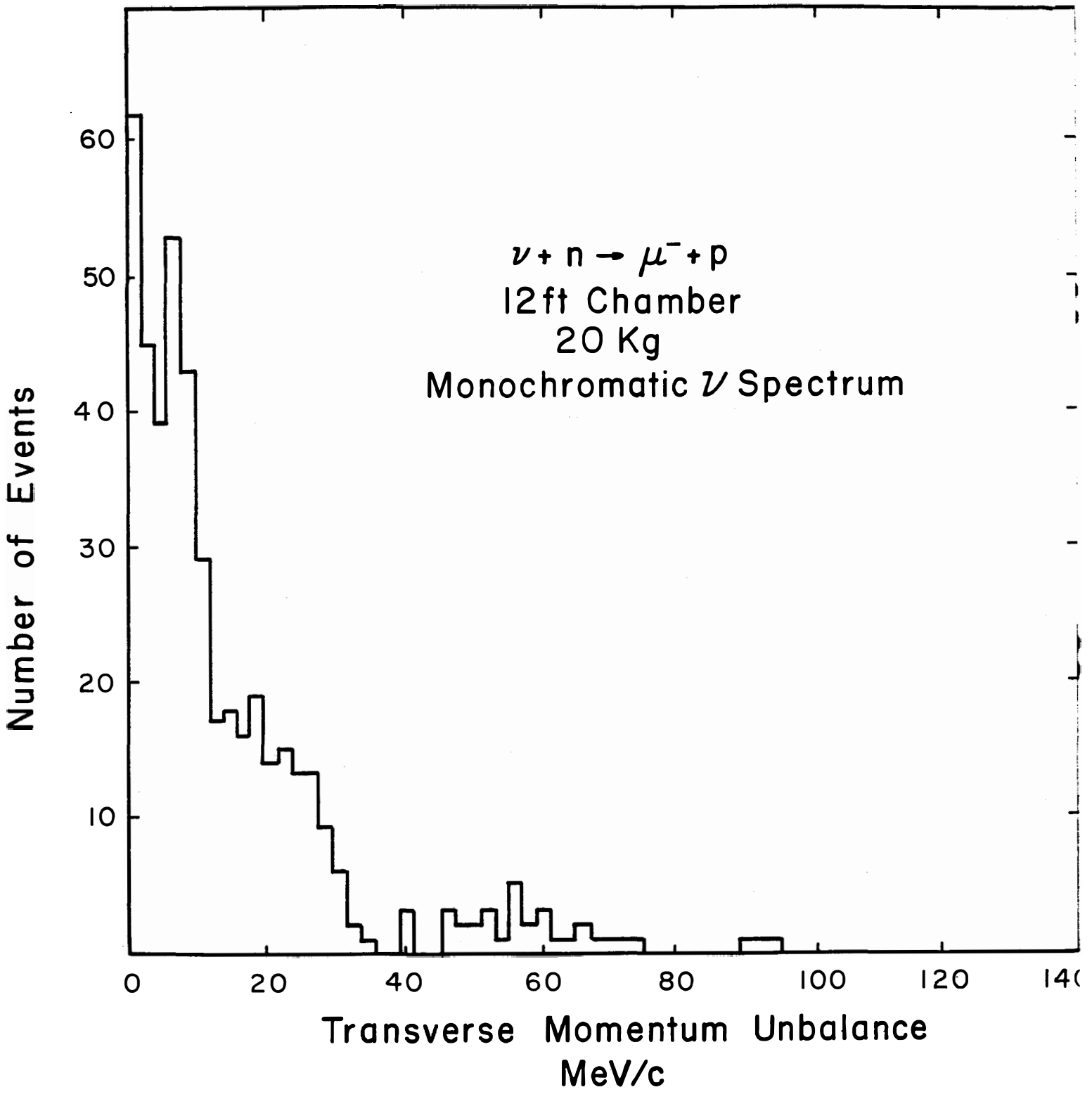

Fig. 6. Missing transverse momentum for elastic events.

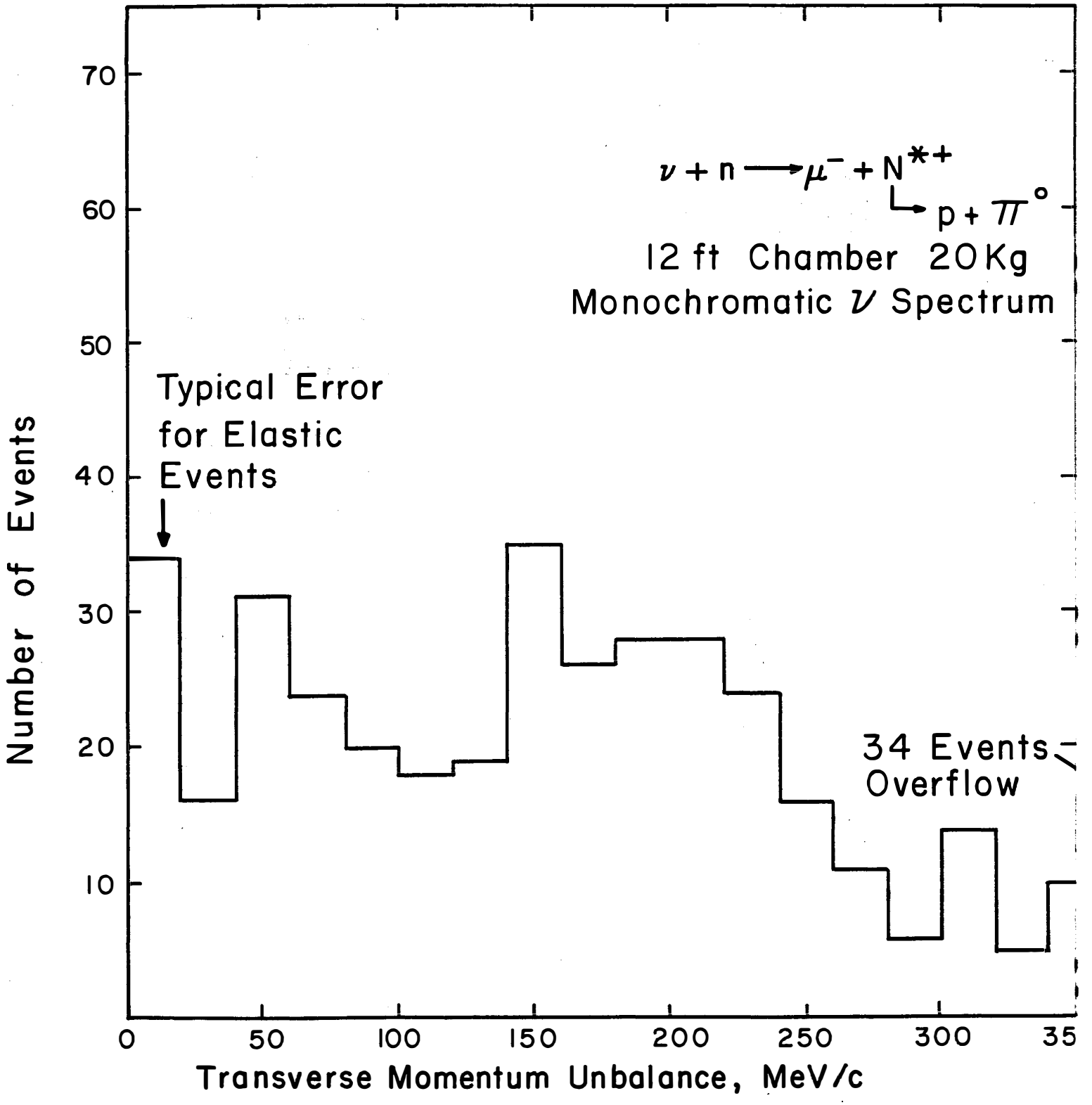

Fig. 7. Missing transverse momentum for inelastic events.

A. 1-68-89-II
July 20, 1968

TM-151
2610.2
2630.2

FAKE STUDIES OF SOME STRONG AND WEAK INTERACTIONS IN THE 12-FT AND 25-FT BUBBLE CHAMBERS

PART II. STRONG INTERACTIONS

M. Derrick
Argonne National Laboratory

T. O'Halloran
University of Illinois

and

R. Kraemer
Carnegie-Mellon University

Introduction

The error formulae and the parameters of the chambers are given in Part I of this report which deals with neutrino interactions. The experiments with hadron beams represent a much larger class of possibilities which could not be properly explored because of the limitations of time. The work was concentrated on 4c types since it is obvious that the 1c events will be much more difficult to handle even using neutron recoils or γ-ray conversions in the chamber. We decided to try events of different characteristics including a class dominated by a single fast forward-going track, and so chose elastic scattering. It is of course unlikely that a bubble chamber would be used to study such reactions, but the technique is used extensively now for similar reactions such as $m + B \rightarrow m^* + B$. As a contrast, we also generated a reaction involving six secondary charged particles which is perhaps a more typical final state at high energies.

Strong-Interaction Events Generated

The different types of event that were generated were specifically:

1. $K^- p \rightarrow K^- p$ with a c.m. angular distribution $d\sigma/dt \propto e^{6t}$
2. $\bar{p}p \rightarrow 3\pi^+ 3\pi^-$ with the pions distributed according to phase space in the c.m.
3. $K^- p \rightarrow K^{*-} p$ with a c.m. angular distribution $d\sigma/dt \propto e^{6t}$
   $\downarrow$
   $K^o \pi^-$
   $\downarrow$
   $\pi^+ \pi^-$.

Two of the pions in reaction 2 were constrained to be in a resonance of mass 1 GeV and width 10 MeV with zero spin. The first two reactions were generated at 50 GeV/c, 100 GeV/c, and 200 GeV/c incident-beam momenta, whereas reaction 3 was only studied at 100 GeV/c. In all cases the beam-momentum spread was taken to be $\Delta p/p = \pm 0.1\%$.

The three examples chosen give final states with 2, 6 and 4 prongs. The $K^- p$ elastic events have the characteristic of a single very high momentum forward track which favors the 25-ft chamber since the momentum precision is measurement limited and long tracks are needed.

The 6-prong $\bar{p}p$ annihilations simulate a class of events which could be produced by a multiperipheral process. Such events will probably become more important as the energy increases. Even at present energies, where two-body final states are quite strong, most of the inelastic cross section seems to represent multibody final states.

The same canonical four sets of chamber parameters were used as in the ν study, that is:

(i) 12-ft chamber	20 kG	250μ setting error
(ii) 12-ft chamber	40 kG	250μ setting error
(iii) 25-ft chamber	40 kG	250μ setting error
(iv) 25-ft chamber	40 kG	500μ setting error

K^-p ELASTIC SCATTERING

Results from FAKE

In Table I we show the results for a typical event at 50 GeV/c in the four chambers. About 60% of the protons stop in the hydrogen (12 ft, 40 kG) which is a great advantage of these big chambers. Figures 1-3 show the momentum precision on the secondary kaon track as a function of track length for 50, 100, and 200 GeV. In all cases the scattered kaon has nearly the same momentum as the beam. The long tracks are multiple-scattering limited, and it is clear that the 25-ft chamber has tracks in this regime even up to 200 GeV. Comparing cases (ii) and (iv) at 50 GeV/c, the ultimate precision is about the same provided one allows 3 m of secondary track in the 12-ft chamber. At 200 GeV/c, however, the 12-ft chamber is clearly getting too small for this kind of event, and even the 25 ft is being pushed to its limits.

The accuracy of momentum measurement on this track obviously dominates the situation. The beam-momentum spread of 0.1% is negligible in comparison. For this particular type of event then a tighter beam momentum spread will not help the kinematics.

The transverse momentum unbalance (ΔP_T) is shown in Figs. 4

Table I. FAKE Results for a Typical Event $K^- p \rightarrow K^- p$
At 50 GeV/c in the Four-Chamber Parameter Combinations.

		X	Y	Z	DX	DY	DZ				
Vertex coordinates		-141.22	6.64	-99.95	0.025	0.025	0.025				
								Chamber (a) 12 ft, 40 kG, 250μ			
			Millirad								
		MeV/c			Errors			Cm		Micron	
Track	Charge	P	Dip	Phi	ΔP	Δλ	Δφ	Length	+-	Sagitta	
1	-	139162	-0	3141	176661	1	3	-51.03	0.05	140	interacts
2	-	50235	-2	6282	557	0	0	333.33	0.05	-16588	
3	+	376	254	1363	8	14	20	32.21	0.10	20013	stops
		X	Y	Z	DX	DY	DZ				
Vertex coordinates		-141.22	6.80	-99.95	0.025	0.025	0.035				
								Chamber (b) 12 ft, 40 kG, 250μ			
1	-	43545	-0	3147	24675	1	3	-51.03	0.05	531	interacts
2	-	50070	-2	5	287	0	0	332.87	0.05	-33194	
3	+	378	254	1369	4	14	20	32.21	0.10	39850	stops
		X	Y	Z	DX	DY	DZ				
Vertex coordinates		-315.93	7.33	-149.92	0.025	0.025	0.052				
								Chamber (c) 25 ft, 40 kG, 500μ			
1	-	56598	-0	3158	5400	1	2	-83.98	0.05	1869	interacts
2	-	49862	-2	13	91	0	0	712.75	0.05	-152828	
3	+	378	256	1377	4	14	20	32.20	0.10	39814	stops
		X	Y		DX	DY	DZ				
Vertex coordinates		-315.89	7.29	-149.84	0.050	0.050	0.104				
								Chamber (d) 25 ft, 40 kG, 500μ			
1	-	65450	-1	3154	14434	2	4	-83.98	0.10	1616	interacts
2	-	49931	-2	13	136	0	0	712.78	0.10	-152628	
3	+	380	261	1370	5	15	21	32.21	0.20	39599	stops

TM-151
2610.2
2630.2

and 5 for the 50 GeV/c and 200 GeV/c cases. This variable is dominated by the recoil proton so the change with beam momentum is not strong. All cases are comparable with ΔP_T approximately 50 MeV/c for 50 GeV and 100 MeV/c for 200 GeV. The beam momentum spread of 0.1% $\Delta p/p$ together with the much larger $\Delta p/p$ on the secondary track (Figs. 1-3) give a longitudinal momentum unbalance (ΔP_L) that increases faster than the momentum. The ΔP_L comes from the secondary-kaon track and is typically 250 MeV/c for 50 GeV and 1400 MeV/c for 200 GeV for case (iv) and twice as large for case (ii) for events in the fiducial region which we take to be the upstream half of the chamber.

The total c.m. energy for events occurring in the fiducial volume is shown in Figs. 6-8 for the three beam momenta. On each figure a scale of 280 MeV (± 1 π^o mass) is shown for comparison. At the lowest momentum the width of the distributions is quite tight with a full width in the range 50 to 100 MeV with chambers (ii) and (iv) comparable, whereas at 200 GeV the resolution is becoming marginal and only the 25-ft chamber with 250μ setting error has nearly enough accuracy. At 100 GeV/c case (iv) still gives a tight distribution, whereas the 12-ft chamber with 20 kG is clearly inadequate.

Results of Fitting

The results of fitting, about 50 such events for each momentum and chamber combination are summarized in Table II. The events listed in the Table are just those with primary vertex in the upstream half of the chamber.

Table II. Results of Fitting a Small Number of Events for each Combination.

Beam Momentum GeV/c	Chamber size feet	Chamber B Field kG	ϵ	Total Events	Unique Fits	2-Fold Ambiguous Fits	3-Fold Ambiguous Fits
50	12	20	250	23	14	8	1
50	12	40	250	23	15	8	0
50	25	40	250	28	24	3	1
50	25	40	500	28	24	4	0
100	12	20	250	27	10	13	4
100	12	40	250	27	13	11	3
100	25	40	250	29	20	8	1
100	25	40	500	29	18	9	2

All events were ambiguous with πp or pp elastic scattering but this was neglected. Assuming the incident beam to be pure kaons, then the hypotheses tried were

(i) $K^- p \rightarrow K^- p$ generated

(ii) $K^- p \rightarrow K^- p \pi^o$

(iii) $K^- p \rightarrow \pi^- p \bar{K}^o$ with the $\bar{K}^o$ missing

(iv) $K^- p \rightarrow K^- \pi^+ n$.

The column labeled 2-fold ambiguous means that one of the hypotheses, (ii), (iii), or (iv), gave a fit (with χ^2 probability > 1%) in addition to the elastic fit. The 3-fold ambiguous events gave fits to two of the three inelastic hypotheses in addition to the elastic fit.

At 200 GeV/c there was evidence that the fitting program had some convergence problems, so the results are unreliable and are not given.

The results are encouraging and support the conclusions one would draw from the FAKE data presented earlier. The fraction of ambiguities is quite similar to those obtained today in smaller

chambers with lower-momentum beams. The 25-ft chamber is clearly superior to the 12 ft because of the extra track length available and can be used for this kind of experiment to somewhere beyond 100 GeV but less than 200 GeV, whereas the 12-ft chamber probably cuts out below 100 GeV/c.

$\bar{p}p$ ANNIHILATIONS TO SIX-CHARGED PIONS

Results from FAKE

The results for this final state are quite different from the elastic scattering. The momentum spectrum of the pions for 100-GeV incident antiprotons is shown in Fig. 9. The average momentum is about 13 GeV/c as expected (100/6) with very few tracks having momenta greater than 50 GeV/c. The tracks are peaked forward at all energies, in general coming out within a cone of approximately 18° half angle at 100 GeV/c (see Fig. 10).

The relatively low momentum of the secondary tracks combined with a 40 kG field spreads out the pions so they leave the chambers over a large fraction of the downstream wall, as can be seen in Fig. 11 which shows the end points of all the tracks, including the beam antiproton for the 12 ft and 25-ft chambers with 40 kG and 100-GeV incident beam momentum. The beam is clearly delineated. Points not on the chamber wall represent tracks that gave a secondary interaction in the hydrogen. Any neutral pions produced in the reaction would fall inside the 18° cone and the γ rays from the π^o decays will only widen this distribution by a few degrees. It is clear then that any region in the downstream part of

the chamber for γ-ray conversion will also intersect a large fraction of the secondary-pion tracks. These secondary pions will give many interactions in the neon or plate region and lead to great confusion in scanning for γ rays from the primary vertex.

Table III gives the FAKE printout for a typical event at 100 GeV/c in the four chamber combinations. The beam momentum is unmeasured in all cases since the beam track is very short. The third secondary track interacts and, for the 25-ft chamber, so also does the first secondary track. Chambers (ii) and (iv) have comparable errors.

The momentum precision on the secondary tracks for the four chambers at the three energies is shown in Figs. 12-14. The values now cover a wide band, since the annihilation pions cover a wide momentum spectrum unlike the scattered kaons in the previous reaction. For the $\bar{p}p$ annihilation the 12-ft chamber with 40 kG has a region with tracks which are scattering limited even as high as 100 GeV/c, whereas at 200 GeV/c only the 25-ft chamber is long enough. At 50 GeV the chambers are comparable in accuracy for the longest tracks.

At 100 GeV/c the long tracks give $\Delta p/p$ in the range 0.3% to 0.6% for cases (ii) 12 ft, 40 kG, 250μ and (iv) 25 ft, 40 kG, 500μ. Since the mean momentum of the pions is 6 times lower than the beam, a beam-momentum spread of 0.05% to 0.1% is required to match the error per track. Since there are six secondary particles, a beam momentum spread of 0.1% is adequate.

The last two pions of the six were made in a resonance of mass

Table III. FAKE Results for a Typical Event $\bar{p}p \rightarrow 3\pi^+ 3\pi^-$
At 100 GeV/c in the Four-Chamber Parameter Combinations.

		X	Y	Z	DX	DY	DZ				
Vertex coordinates		-181.15	-1.76	-99.98	0.025	0.025	0.035				
								Chamber (a) 12 ft, 20 kG, 250μ			
			Millirad								
		MeV/c				Errors		Cm		Micron	
Track	Charge	P	Dip	Phi	ΔP	Δλ	Δφ	Length	+-	Sagitta	
1	-	10022	1	3148	18779	6	13	-11.27	0.05	95	interacts beam
2	+	31998	91	111	213	0	0	374.48	0.07	32735	
3	+	2164	303	416	9	2	3	337.06	0.11	375675	
4	-	11647	-5	6262	120	0	1	178.43	0.05	-20500	interacts
5	-	30960	-27	6197	202	0	0	373.16	0.06	-33721	
6	+	18608	-129	6216	94	0	0	373.66	0.08	55809	
7	-	5643	-46	6256	22	1	1	371.99	0.06	-183706	
		X	Y	Z	DX	DY	DZ				
Vertex coordinates		-181.15	-1.75	-99.98	0.025	0.025	0.035				
								Chamber (b) 12 ft, 40 kG, 250μ			
1	-	18224	1	3149	31038	6	13	-11.27	0.05	105	interacts beam
2	+	32032	91	111	107	0	0	375.30	0.07	65687	
3	+	2167	303	416	5	2	3	337.06	0.11	750375	
4	-	11689	-5	6263	60	0	1	178.43	0.05	-40853	interacts
5	-	30921	-27	6197	101	0	0	373.95	0.06	-67814	
6	+	18616	-129	6217	47	0	0	370.88	0.08	109920	
7	-	5667	-46	6256	11	1	1	362.03	0.06	-346560	
		X	Y	Z	DX	DY	DZ				
Vertex coordinates		-381.78	-1.74	-99.96	0.025	0.025	0.062				
								Chamber (c) 25 ft, 40 kG, 250μ			
1	-	36942	1	3147	48655	8	8	-18.25	0.05	135	interacts beam
2	+	32053	91	112	72	0	0	503.07	0.07	117943	interacts
3	+	2167	303	417	5	2	3	337.06	0.11	750365	
4	-	11689	-5	6263	60	1	1	178.43	0.05	-40854	interacts
5	-	30875	-27	6198	45	0	0	783.65	0.06	-298242	
6	+	18606	-129	6217	26	0	0	759.05	0.08	460640	
7	-	5673	-45	6258	8	1	1	673.02	0.06	-1196285	

TM-151
2610.2
2630.2

Table III. (Continued)

	X	Y	Z	DX	DY	DZ
Vertex coordinates	-381.76	-1.69	-99.91	0.025	0.025	0.025

Chamber (d) 25 ft, 40 kG, 500μ

Track	Charge	MeV/c P	Millirad Dip	Millirad Phi	Errors ΔP	Errors Δλ	Errors Δφ	Cm Length	+-	Micron Sagitta		
1	-	22675	3	3151	36436	16	17	-18.31	0.10	222	interacts	beam
2	+	32022	91	112	110	5	1	505.12	0.14	118078	interacts	
3	+	2167	303	417	5	2	3	336.99	0.21	750045		
4	-	11647	-4	6264	106	2	2	178.36	0.10	-40969	interacts	
5	-	30891	-26	6198	55	0	0	783.65	0.11	-298087		
6	+	18612	-128	6217	29	0	1	759.12	0.15	460597		
7	-	5673	-45	6257	8	1	1	673.10	0.12	-1196612		

TM-151
2610.2
2630.2

1 GeV and width 10 MeV. The effective mass plot of these two particles for the 50 GeV and 200-GeV beam momenta is shown in Figs. 15 and 16. There is very little to choose between the different chambers in this variable and the variation with beam momentum is not strong, probably because angle errors are very important for this low a mass resonance (see Derrick and Kraemer's report on optimum magnetic fields). In all cases the width is to 40 MeV, which means resonance-mass resolution will not be a serious problem for most experiments.

The total c.m. energy as measured from the secondary pions only is shown in Figs. 17-19 for events occurring upstream in the chambers. At 50 GeV/c the distributions are less than 100 MeV wide and this is maintained for the three chamber examples with 40-kG magnetic fields at 100 GeV. At 200-GeV incident momentum the widths have approximately doubled and the discrimination against an additional π^o is becoming marginal, except for case (iii) 25 ft, 250μ. The events not in the central peak come from those with pion tracks shortened by secondary interactions.

Secondary Interactions

For 100 GeV the six pion annihilations were generated with two values of the πp cross section of 25 mb and 50 mb which simulate a hydrogen and deuterium filling of the chamber. All the remaining events discussed in this report were generated with a secondary cross section of 25 mb. The number of events having 1 to 6 secondary tracks interacting is shown in Fig. 20. For a hydrogen filling about half the

secondary tracks interact before leaving the chamber for the case of the 25 ft, whereas for deuterium two-thirds interact. This has two bad effects. First, it clutters up the picture with unwanted tracks, particularly in the far downstream end, and, second, it restricts the possible track length so the momentum accuracy suffers. The situation clearly gets worse as the multiplicity increases, and it will probably be necessary to operate the chambers with only one or two beam tracks. A chamber as large as 25 ft may be too big for this kind of experiment.

The effect on the kinematics can roughly be seen by looking at the total c.m. energy for the events. For the worst case (25-ft chamber, 50 mb) the events having one or two secondary tracks interacting all have the c.m. energy within 100 MeV of the central value whereas only about half the events with more than two tracks interacting fall within that limit. This then reduces the counting rate by about a factor of two. The main problem will be that all events will need measuring since the rejections must be based on kinematic variables rather than on scanning criteria. It is clearly not possible to only accept events in which no secondary track interacts. This points up a major weakness of the bubble-chamber technique if one extrapolates experiments done today to higher energies.

The individual cross sections are decreasing rapidly as the beam energy increases. The larger chambers necessary for measurement accuracy will not increase the event rate as most of the chamber is only needed for measuring the secondary tracks and the increase in

fiducial length will be compensated by the fewer beam tracks that can be used. The secondary interactions further reduce the counting rate. Long runs of the chambers will then be necessary to accumulate enough events.

Results of Fitting

All the events were fit using GRIND. For almost all cases, a fit could be obtained where some $\pi^+\pi^-$ pair was replaced by a K^+K^- pair, so no chamber had sufficient precision to discriminate against this possibility. At lower energies bubble density is used to help this separation, but this is no use at the energies considered here. A small fraction of the events with K pairs could be identified when both kaons interact in the chamber.

The remaining hypotheses were 4c (6 charged pions) and 1c (6 charged pions plus 1 π^o). The fraction of events that gave only a 4c fit are listed in Table IV for events with the primary vertex occurring upstream in the chamber. Additional information could be used to improve these fractions, but even with the numbers given, it seems that this type of event can usefully be studied up to about 200 GeV. Up to 100 GeV the 12-ft chamber with 40 kG and 250μ is as good as the 25-ft chamber with 40 kG and 500μ.

K^* PRODUCTION IN K^-p COLLISIONS

This reaction has been calculated only at 100 GeV/c. The total c.m. energy for the four chambers for events occurring anywhere in

Table IV. $\bar{p}p \rightarrow 3\pi^+ 3\pi^-$.

Beam Momentum	Chamber Combination	% of Events Giving Unique Fits
50 GeV/c ±0.1%	12 ft 20 kG 250μ	68
	12 ft 40 kG 250μ	88
	25 ft 40 kG 500μ	88
	25 ft 40 kG 250μ	90
100 GeV/c ±0.1%	12 ft 20 kG 250μ	50
	12 ft 40 kG 250μ	65
	25 ft 40 kG 500μ	66
	25 ft 40 kG 250μ	76
200 GeV/c ±0.1%	12 ft 20 kG 250μ	31
	12 ft 40 kG 250μ	40
	25 ft 40 kG 500μ	50
	25 ft 40 kG 250μ	50

the chamber, showed no advantage for any chamber. The width was approximately 200 MeV which is worse than the $\bar{p}p$ case at the same energy. The requirement of a visible K^o decay preferentially populates the upstream region of the chamber since all the K^o's go forward.

The transverse-momentum distributions with the K^o ignored are the same for all chambers which says that the P_T unbalance resulting from ignoring the K^o is larger than the uncertainty in P_T coming from the measuring and multiple-scattering error. The P_T distributions were quite similar with only the 25 ft, 40 kG, 250μ being noticeably sharper. The mean uncertainty on P_T was approximately 150 MeV/c which is greater than for the $\bar{p}p$ case probably because the K^o decay-pion tracks were short and not well determined.

The resolution on the K^o mass was about 30 MeV except for case (iii) 25 ft, 40 kG, 250μ, which had a width of about 20 MeV. Angle errors were important for these K^o's as the tracks are short.

The results of fitting the events are summarized in Table V.

Table V. $K^- p \rightarrow K^{*-} p$ at 100 GeV/c ± 0.1%.

$\hookrightarrow K^0 \pi^-$

$\hookrightarrow \pi^+ \pi^-$

Chamber Combination	Total Fits	Unique	Ambiguous 4c best	Ambiguous 1c best	No 4c Fit
12 ft 20 kG 250μ	40	18	13	8	1
12 ft 40 kG 250μ	41	29	5	3	4
25 ft 40 kG 250μ	37	30	3	4	0
25 ft 40 kG 500μ	43	21	10	11	1

The ambiguous column is divided into two sections depending on the relative χ^2 probability of the 4c or 1c fit. The 4c hypothesis was that generated whereas the 1c hypothesis was the final state $p\bar{K}^0\pi^-\pi^0$. The 12-ft chamber with 40 kG (ii) is slightly better than the 25 ft with 500μ setting error (iv) and equally as good as (iii).

Conclusions and Further Studies

This work supports the results of hand calculations and previous computer work in the conclusion that strong-interaction events can be kinematically reconstructed at high energies with the new chambers. The exact upper limit of beam momentum is not sharp but 100 GeV/c seems to be a reasonable value.

For cases having a larger number of charged particles in the final state, a smaller, high-precision chamber is more favored, and for six charged particles the 12-ft chamber is substantially as good as the 25-ft up to 100 GeV/c. Further comparisons of this type should wait on the actual performance of the 7-ft and 12-ft chambers, although further

work on the effect of the setting error, ϵ, would be useful covering the range say from 100μ to 1,000μ. For low-multiplicity events the proposed 25-ft chamber is clearly better than the 12 ft.

If one considers the 12-ft chamber at NAL as a strong-interaction tool, then a field of 40 kG is essential.

An incident beam-momentum bite of ±0.1% is adequate, and smaller values would not add much to the accuracy. This should be specifically checked by generating and fitting some events with different momentum bites in the beam.

This work has shown that events with no missing neutrals do not often give a fit with an additional neutral particle. Since the way 4c events are separated in a bubble-chamber experiment is to ignore any 1c fit ambiguous with a 4c, it is obviously of the first importance to generate some 1c events and see if they give a 4c fit. This should include events in which one of the γ rays from a π^o converted in the hydrogen as a special 2c category.

Acknowledgments

This work was made possible by the help of Denise Pavis at Argonne and Ward Schultz at the University of Colorado.

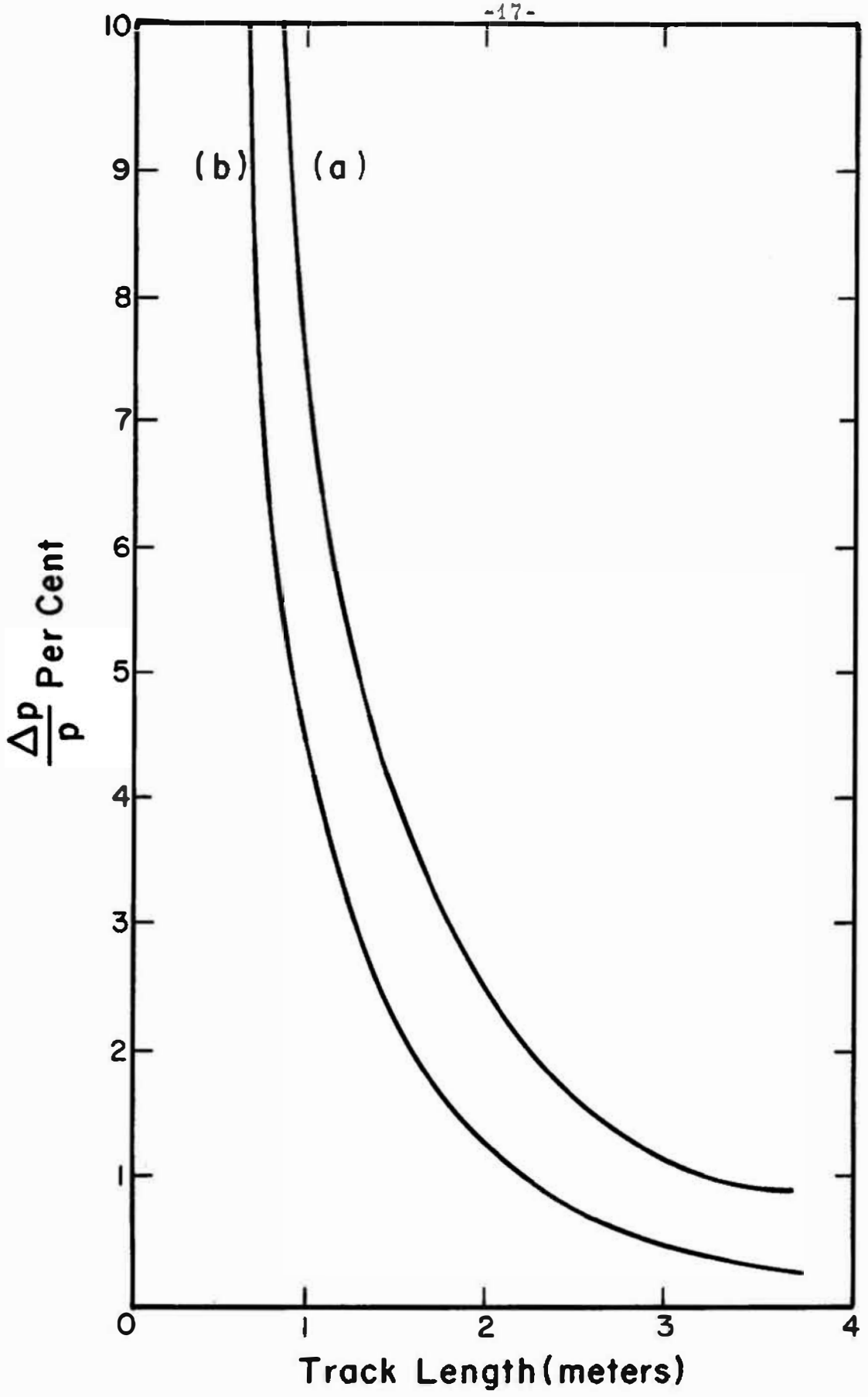

Fig. 1a. FAKE-generated curves of momentum error vs. track length, for the elastic scattering reaction $K^- + p \rightarrow K^- + p$ at 50 Gev/c; this plot is for the ANL 12-ft. chamber, with 20 kgauss magnetic field, setting ε = 250 microns. 1b. Same as 1a, with magnetic field 40 kgauss.

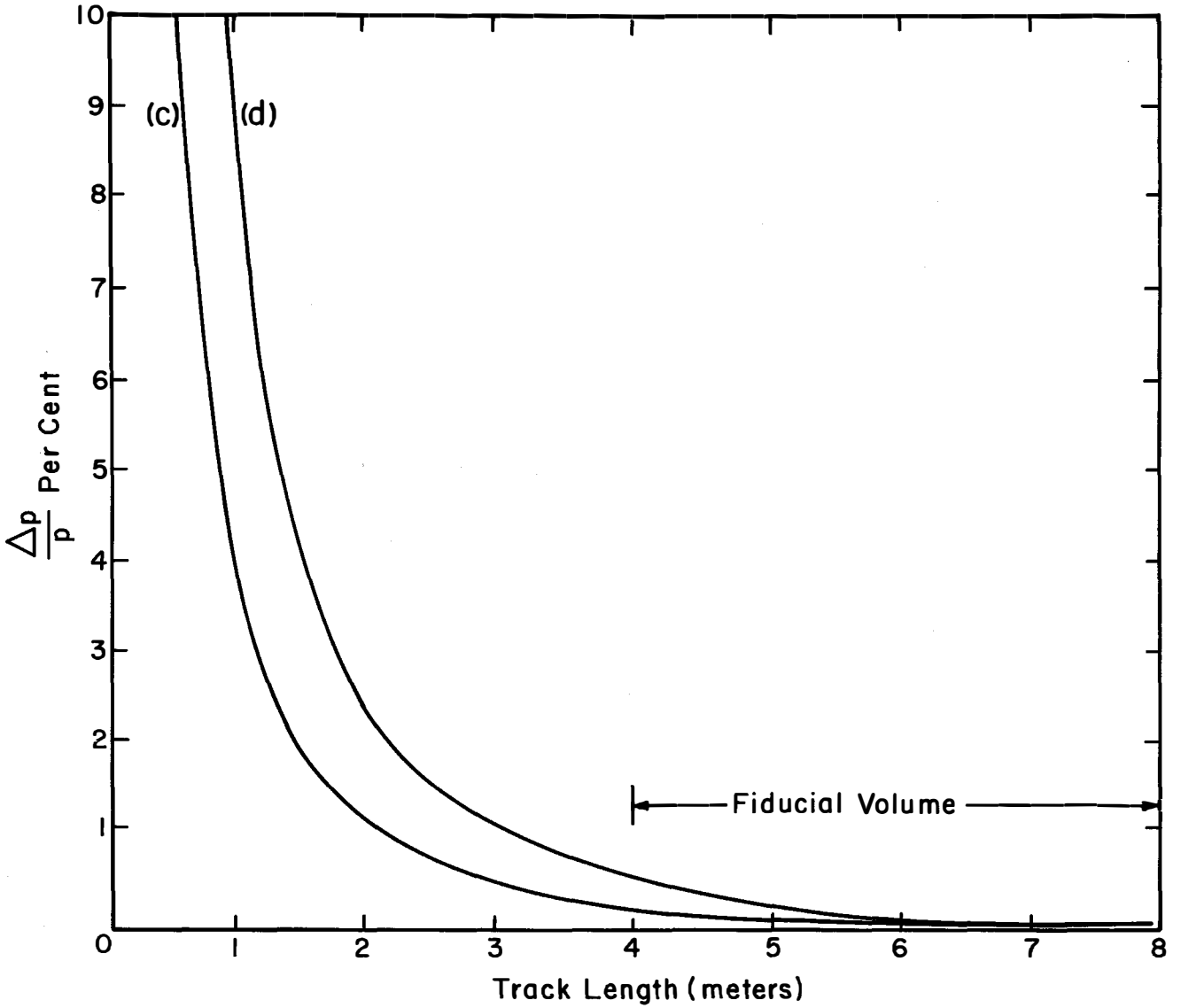

Fig. 1c. Same as 1a, with BNL 25-Ft. chamber, 40 kgauss field, setting error 250μ

Fig. 1d. Same as 1c, but setting error 500μ.

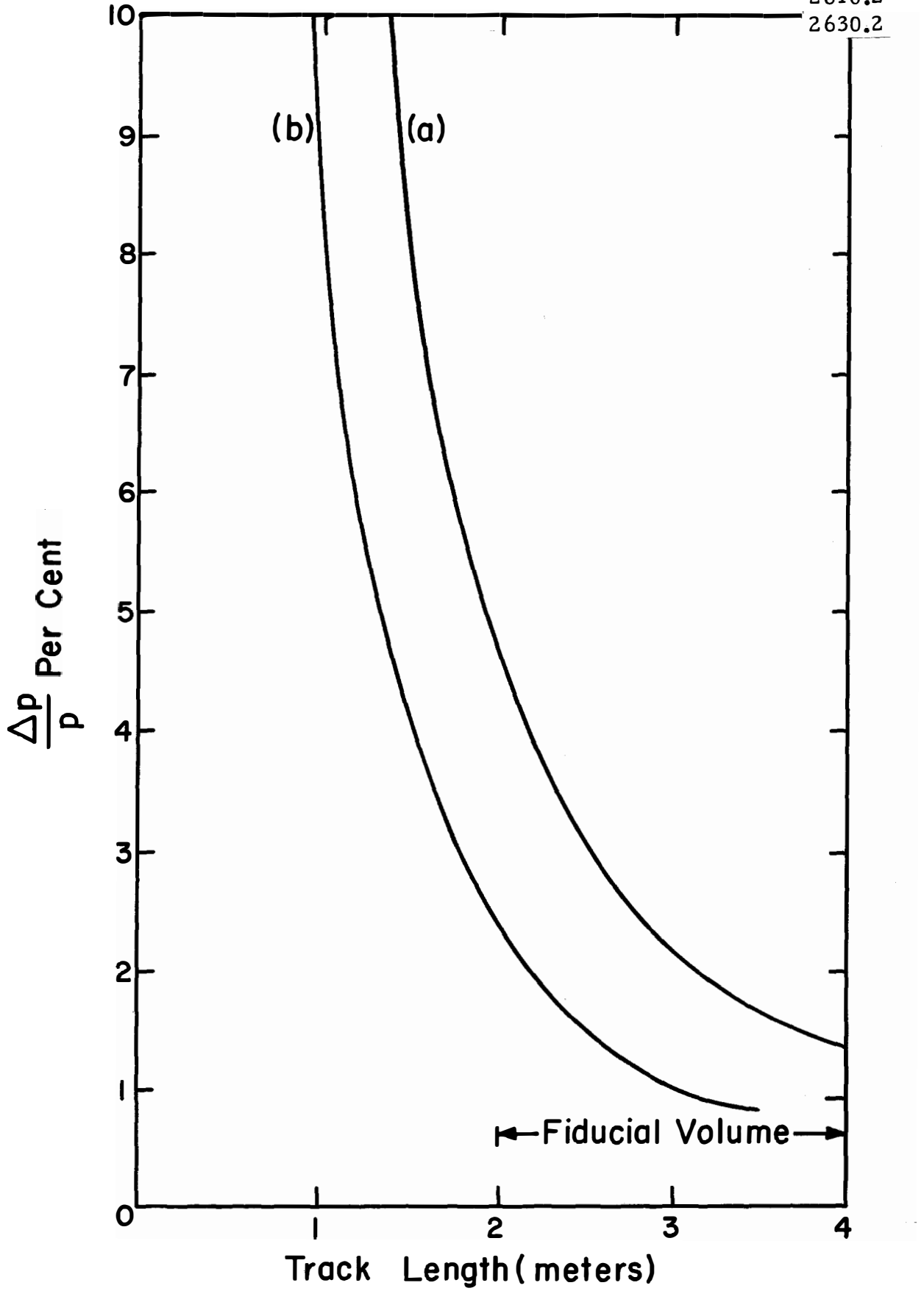

Fig. 2a. Same as 1a, except that K-p scattering is at 100 Gev/c.
2b. Same as 1b, except scattering is at 100 Gev/c.

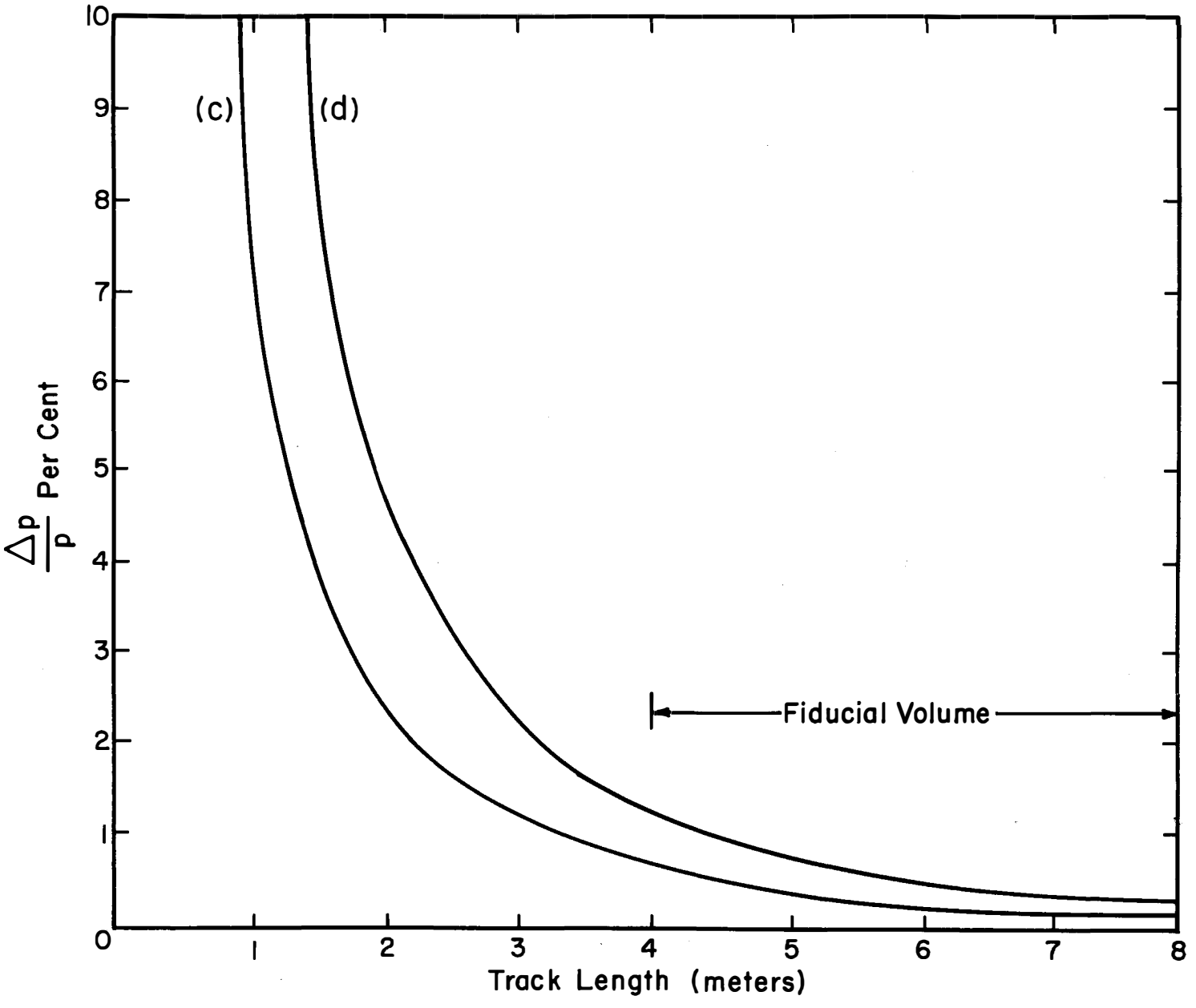

Fig. 2c. Same as 1c, for 100 Gev/c.

Fig. 2d. Same as 1d, for 100 Gev/c.

TM-151
2610.2
2630.2

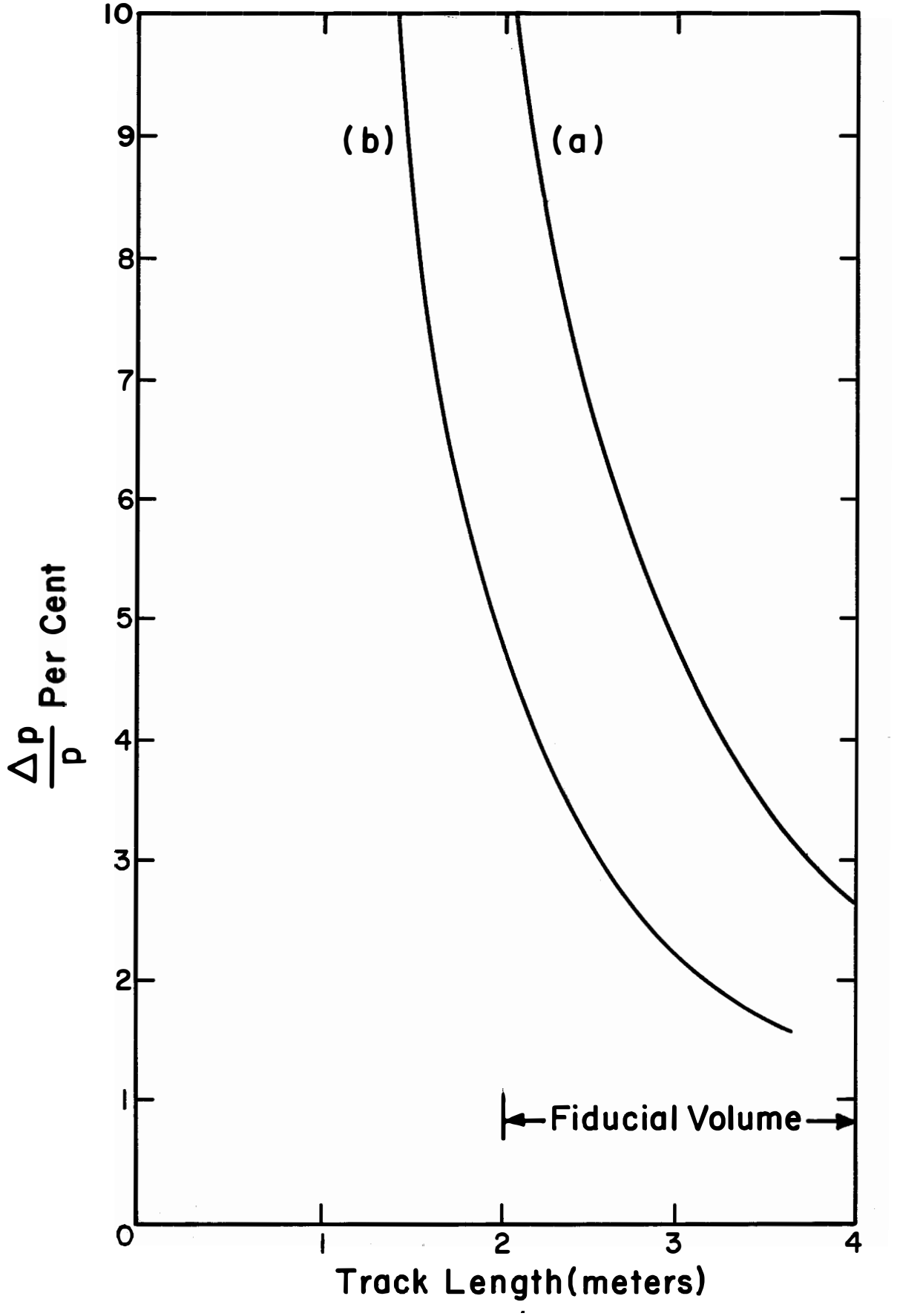

Fig. 3a. Same as 1a, for 200 Gev/c. 3b. Same as 1b, for 200 Gev/c.

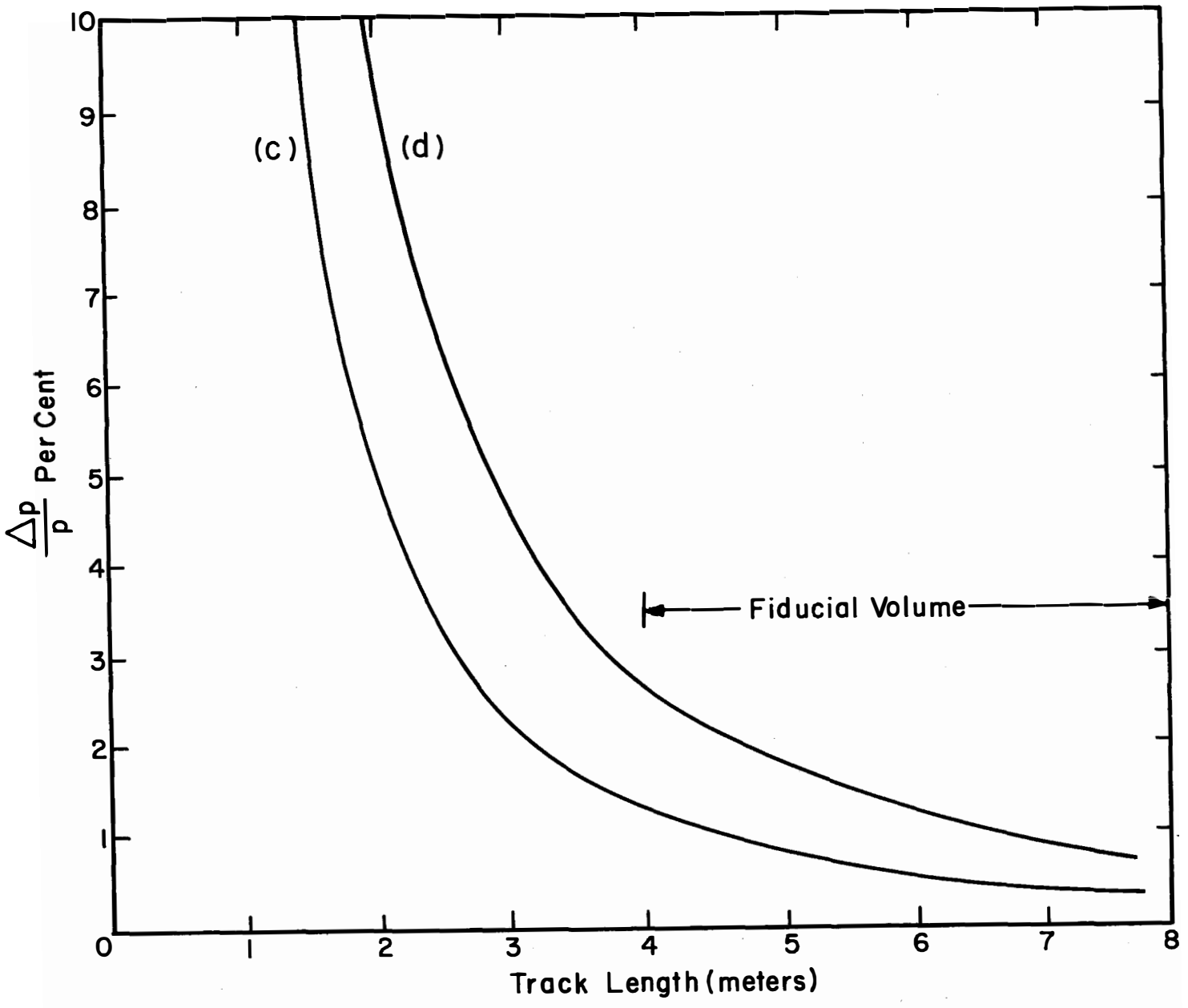

Fig. 3c. Same as 1c, for 200 Gev/c.

Fig. 3d. Same as 1d, for 200 Gev/c.

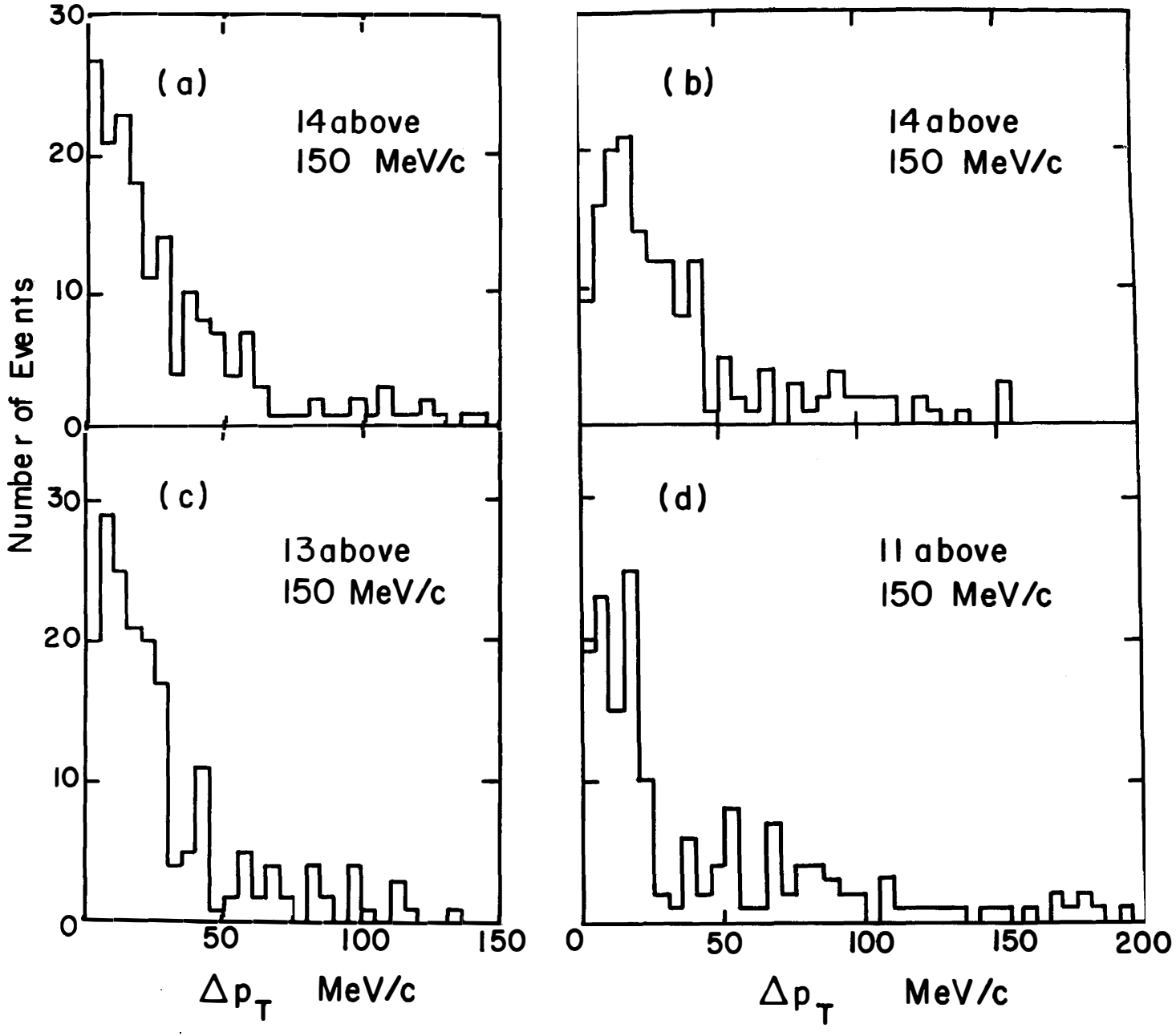

Fig. 4. Spectrum of transverse momentum unbalance for 200 events of K^--p elastic scattering at 50 GeV/c, showing events above 150 MeV/c as overflow. (a) 12-ft chamber, 20-kG field, ϵ = 250μ. (b) Same, with 40 kG. (c) 25-ft chamber, 40 kG, ϵ = 250μ. (d) Same, with ϵ = 500μ.

TM-151
2610.2
2630.2

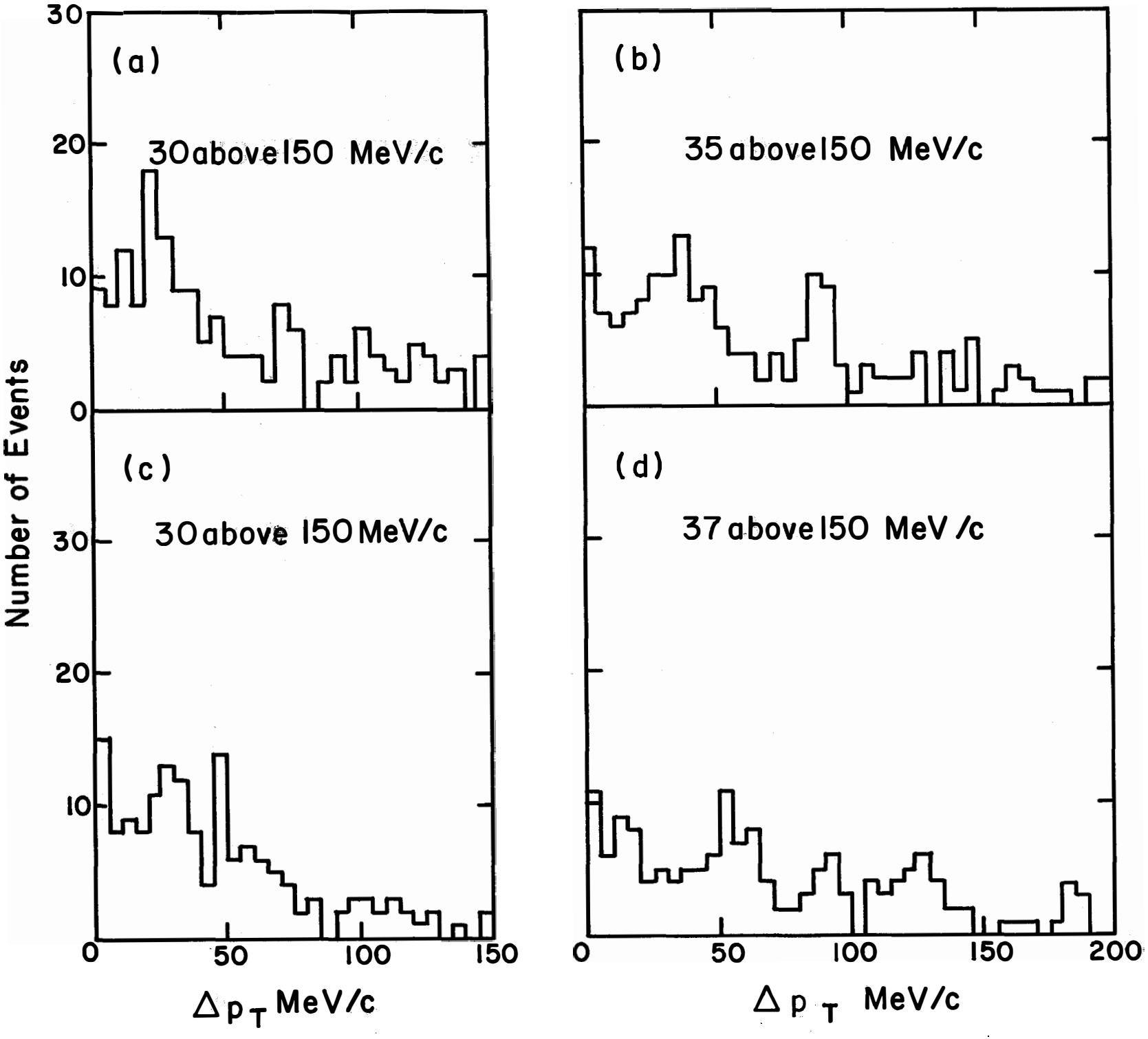

Fig. 5. Same as Fig. 4, except K^--p scattering at 200 Gev/c.

TM-151
2610.2
2630.2

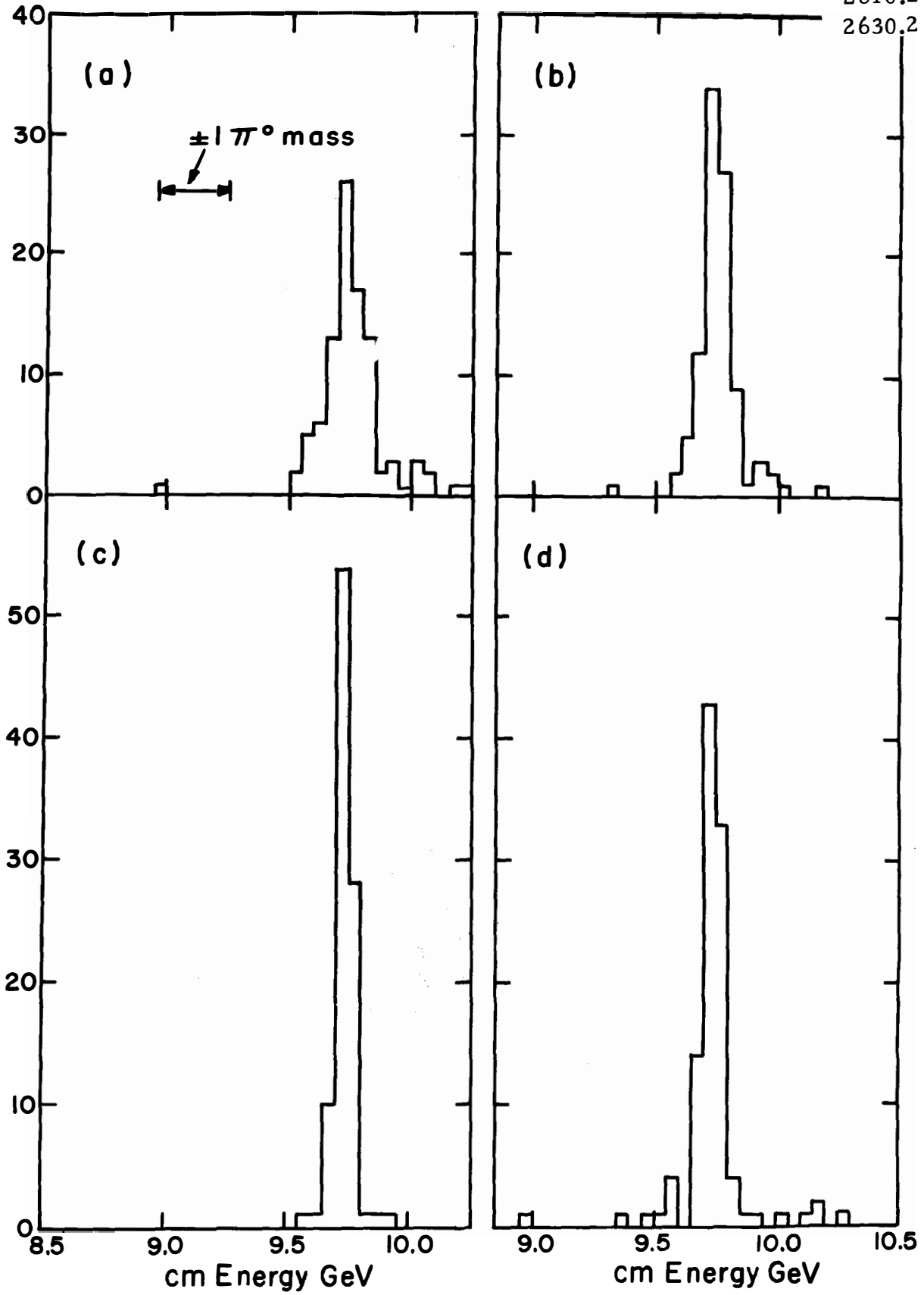

Fig. 6. Resolution in measuring total cm energy, K^--p scattering at 50 GeV/c. Bubble chamber operating conditions as in Fig. 4.

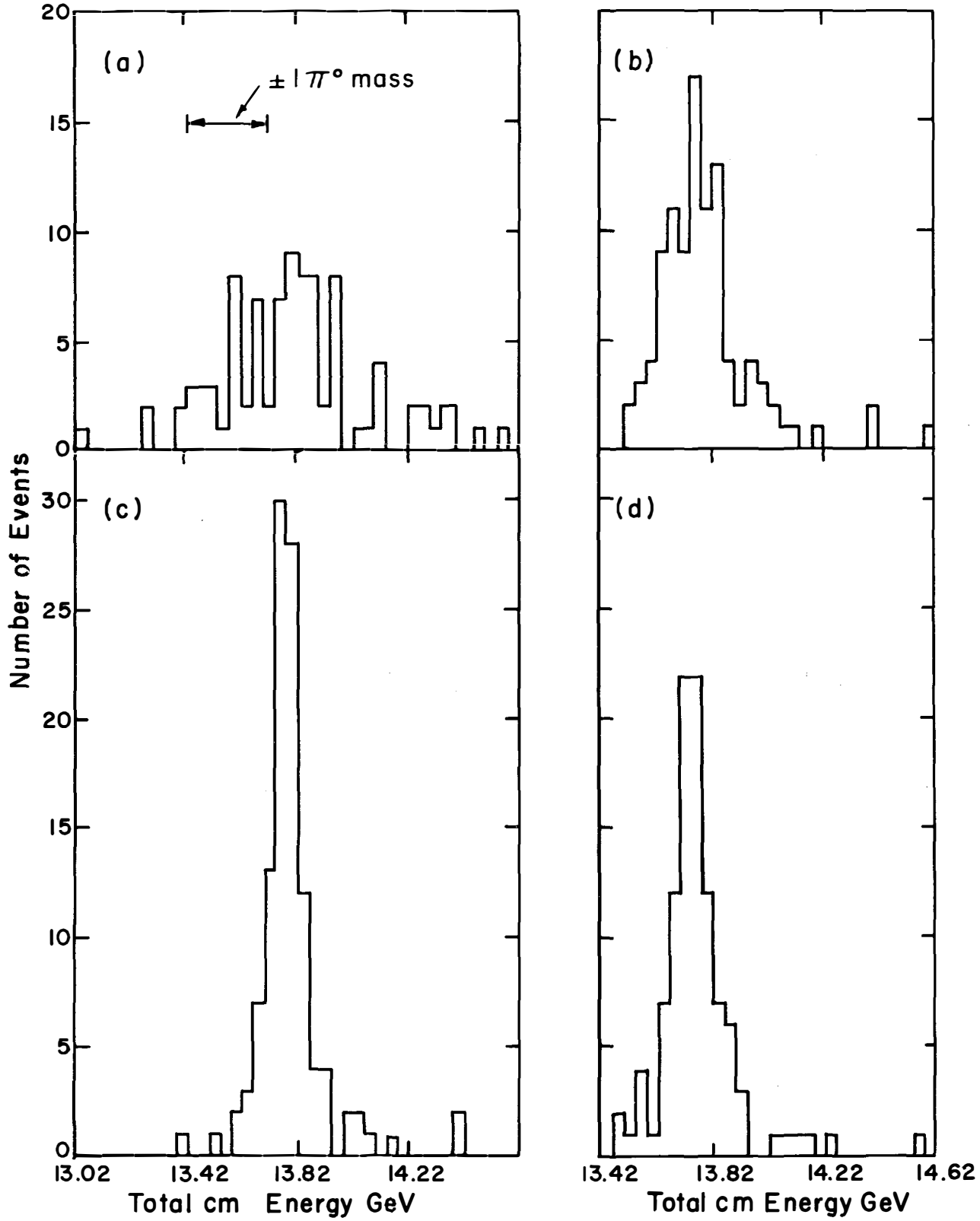

Fig. 7. Same as Fig. 6, at 100 Gev/c.

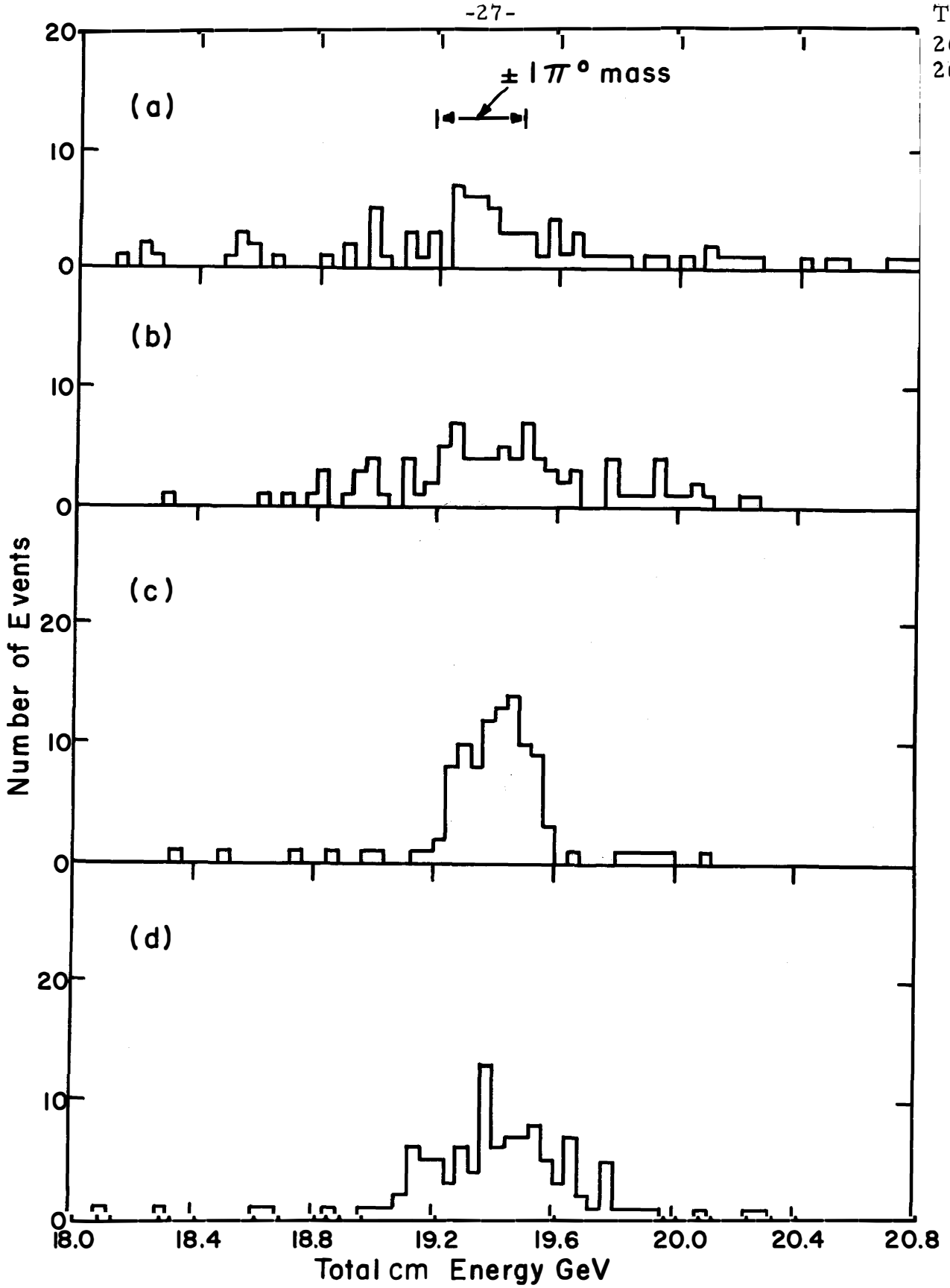

Fig. 8. Same as Fig. 6, at 200 GeV/c.

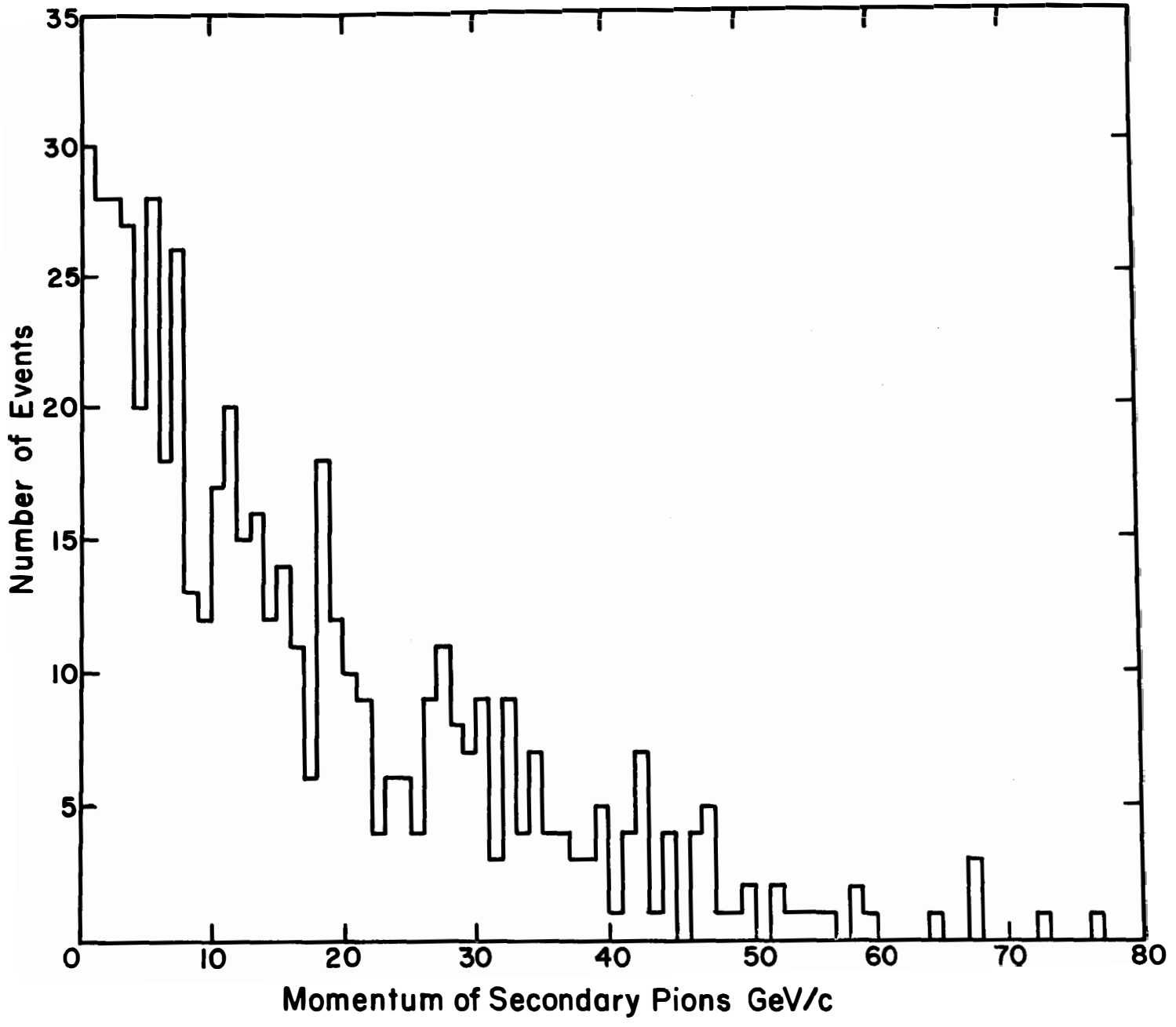

Fig. 9. Distribution of pion momenta given by FAKE for the reaction $\bar{p} + p \rightarrow 3\pi^+ 3\pi^-$ at 100 GeV/c.

TM-151
2610.2
2630.2

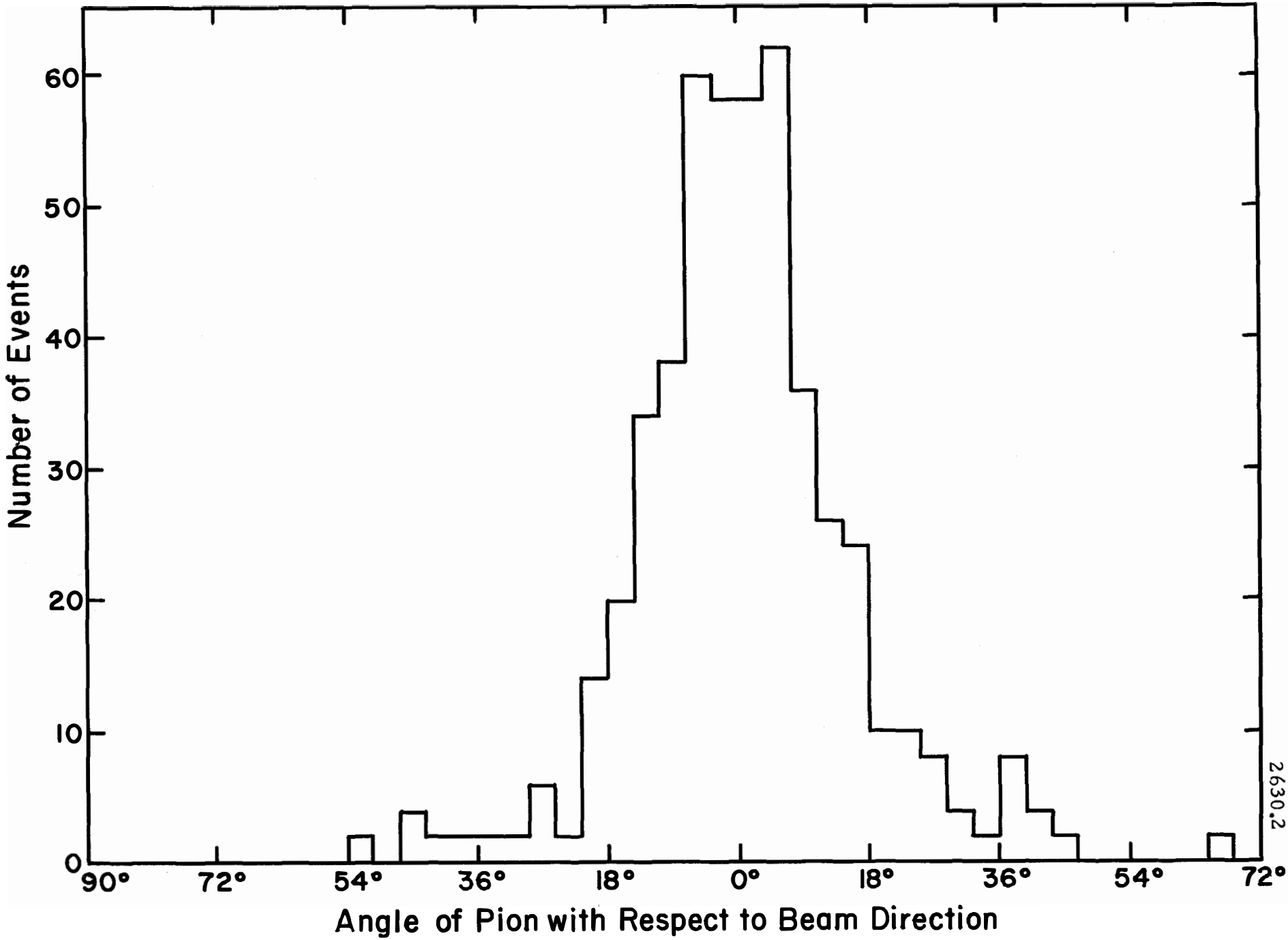

Fig. 10. Angular distribution of pions in the same reaction.

TM-151
2610.2
2630.2

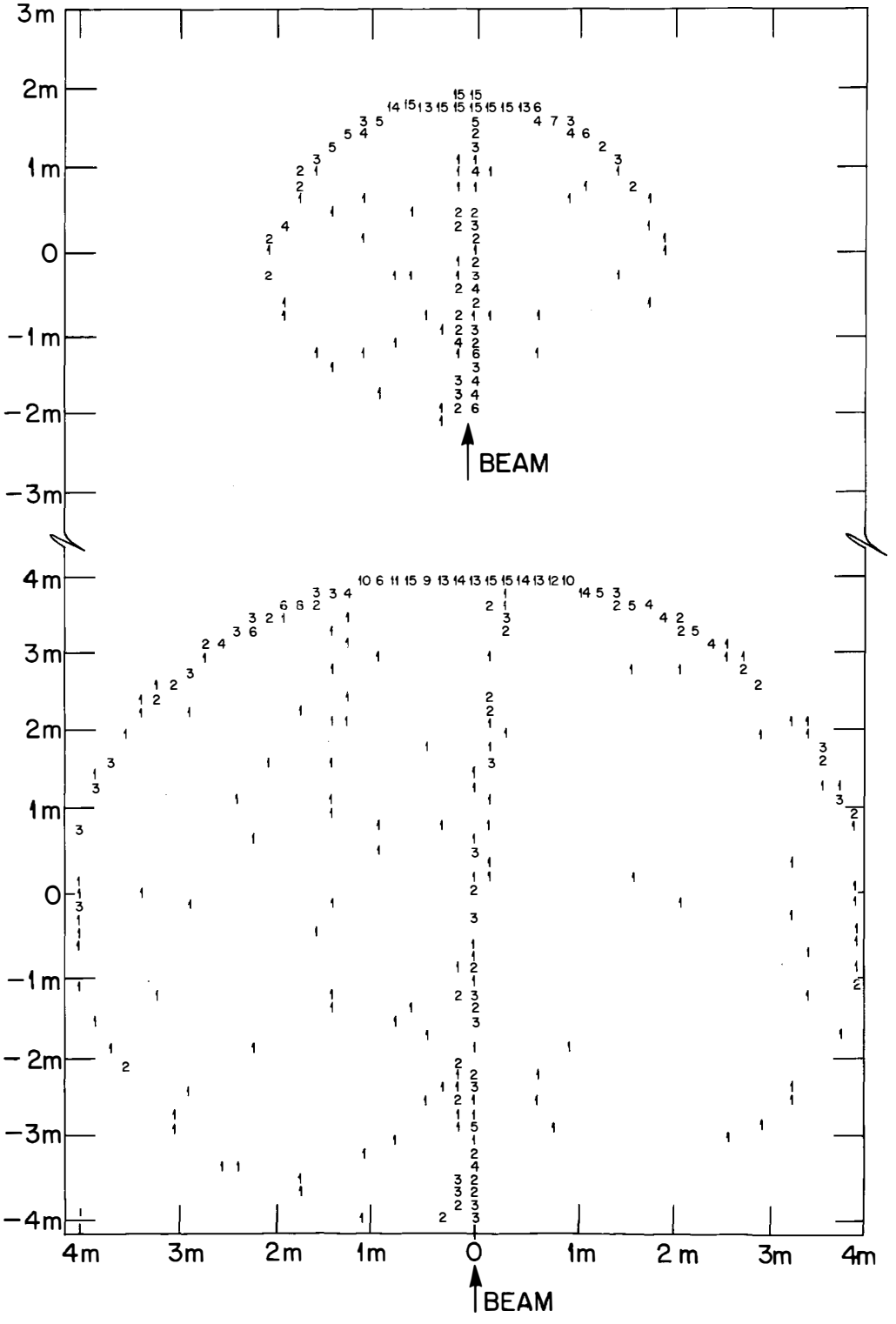

Fig. 11. End points of antiproton and pion tracks in the 12-ft and 25-ft chambers, at 40-kG field. Reaction is $p\bar{p} \rightarrow 3\pi^{+}3\pi^{-}$ at 100 GeV/c.

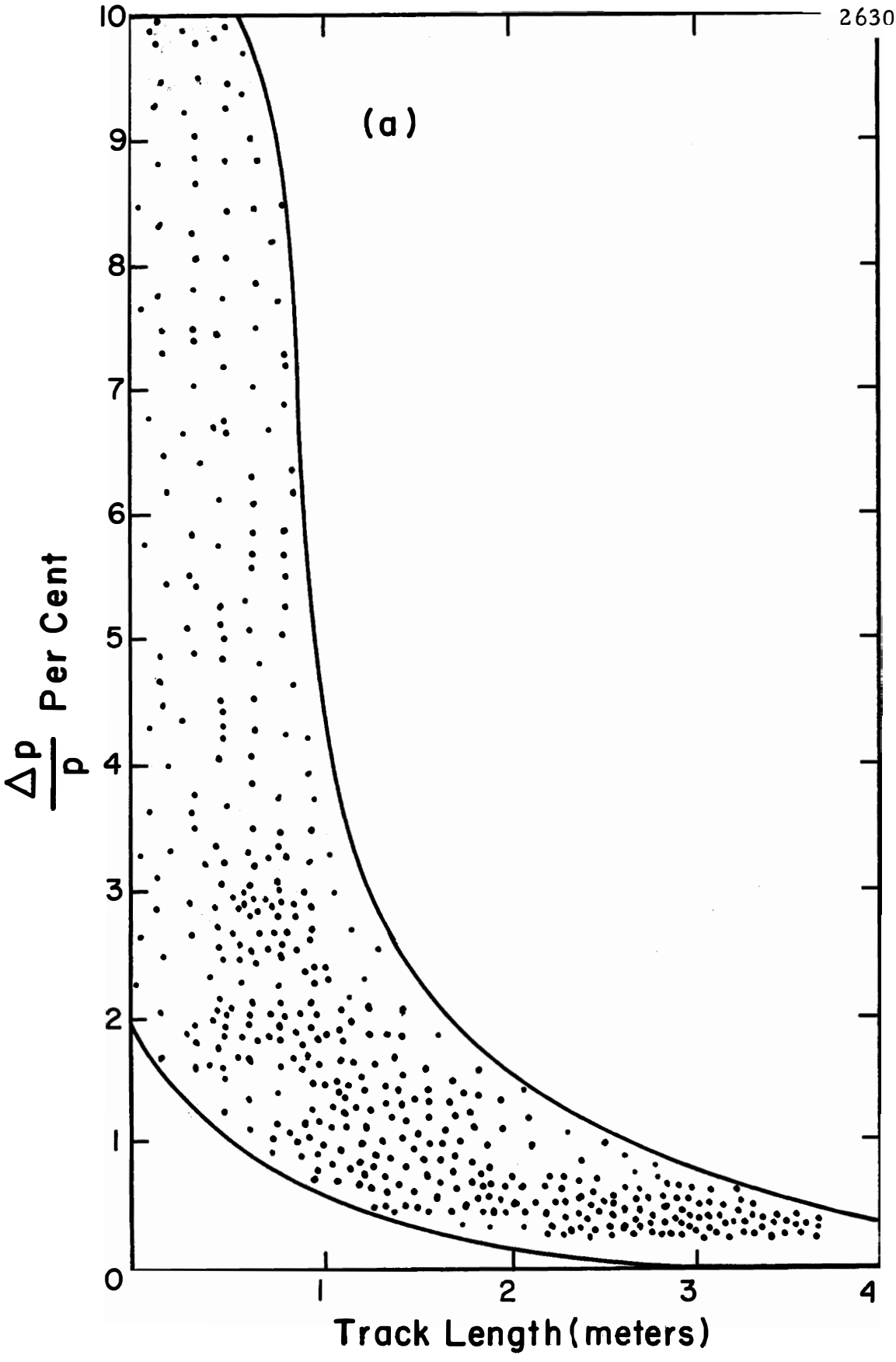

Fig. 12a. FAKE-generated scatter diagram of momentum error vs. track length for the annihilation reaction $\bar{p} + p \rightarrow 3\pi^+ 3\pi^-$ at 50 Gev/c. This plot is for the ANL 12-ft. chamber, 20 kg field, $\varepsilon = 250\mu$.

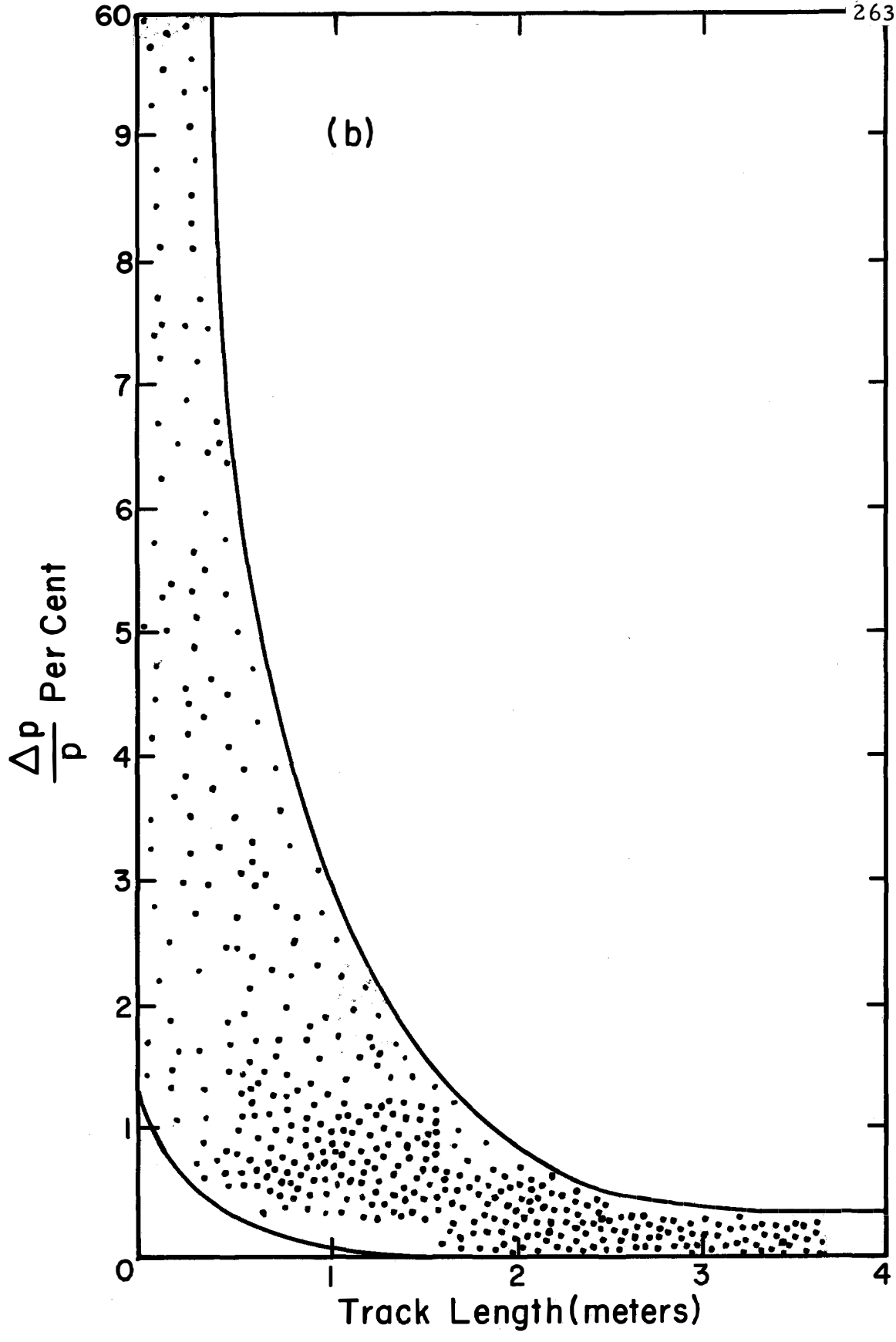

Fig. 12b. Same as 12a, with 40 kgauss field.

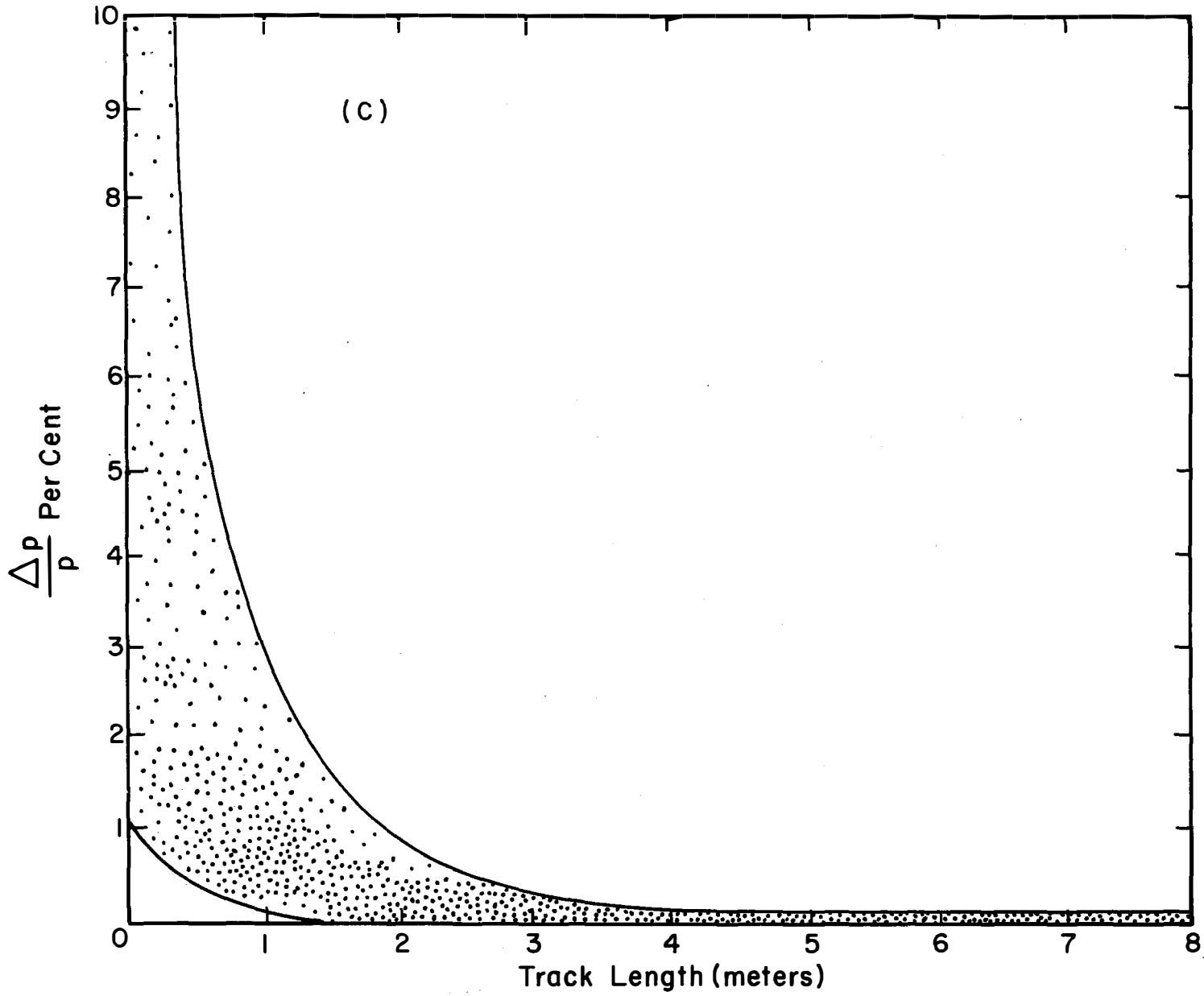

Fig. 12c. Same as 12a, for 25-ft. chamber, 40 kgauss, $\varepsilon = 250\mu$.

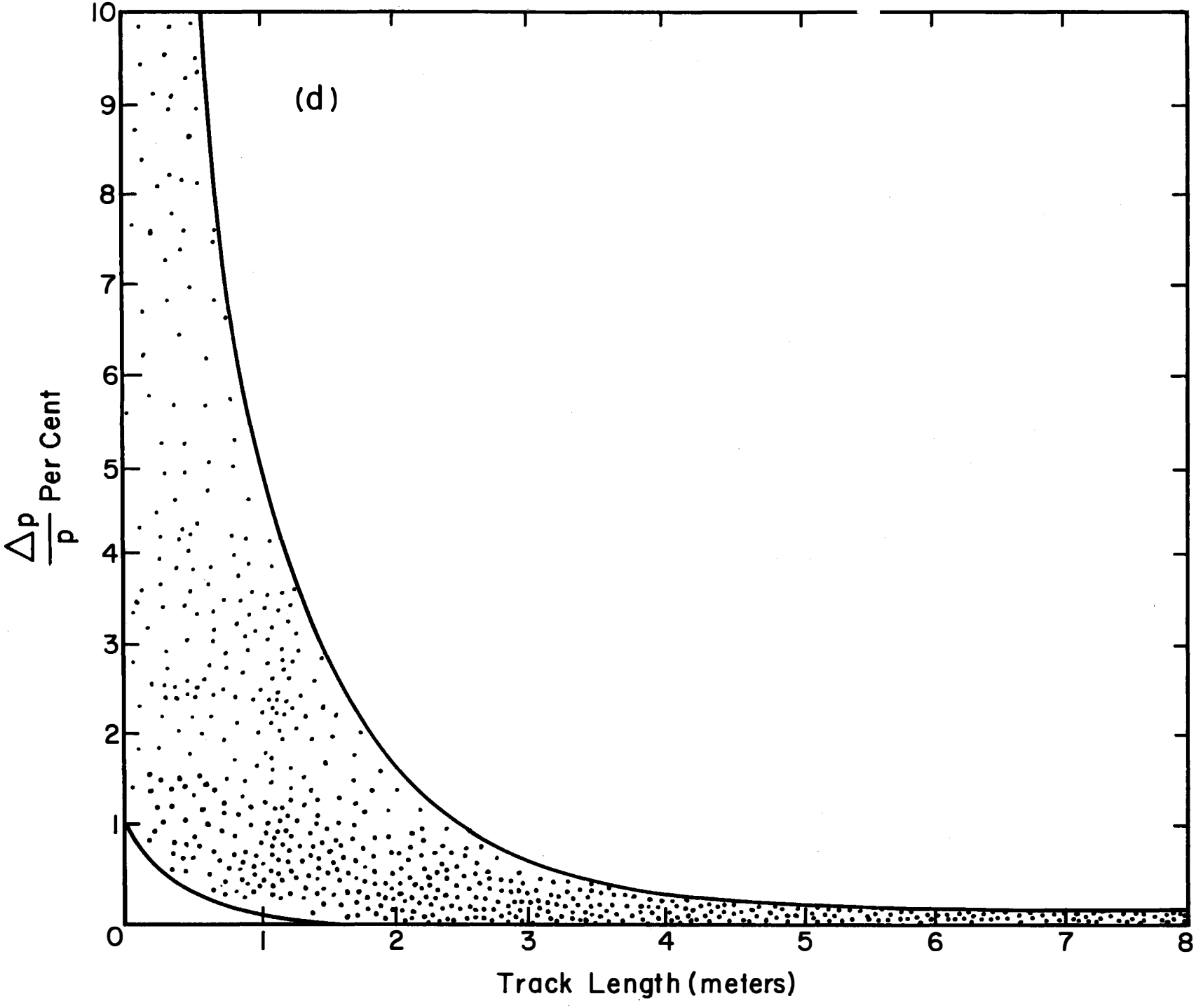

Fig. 12d. Same as 12c, with ε = 500μ

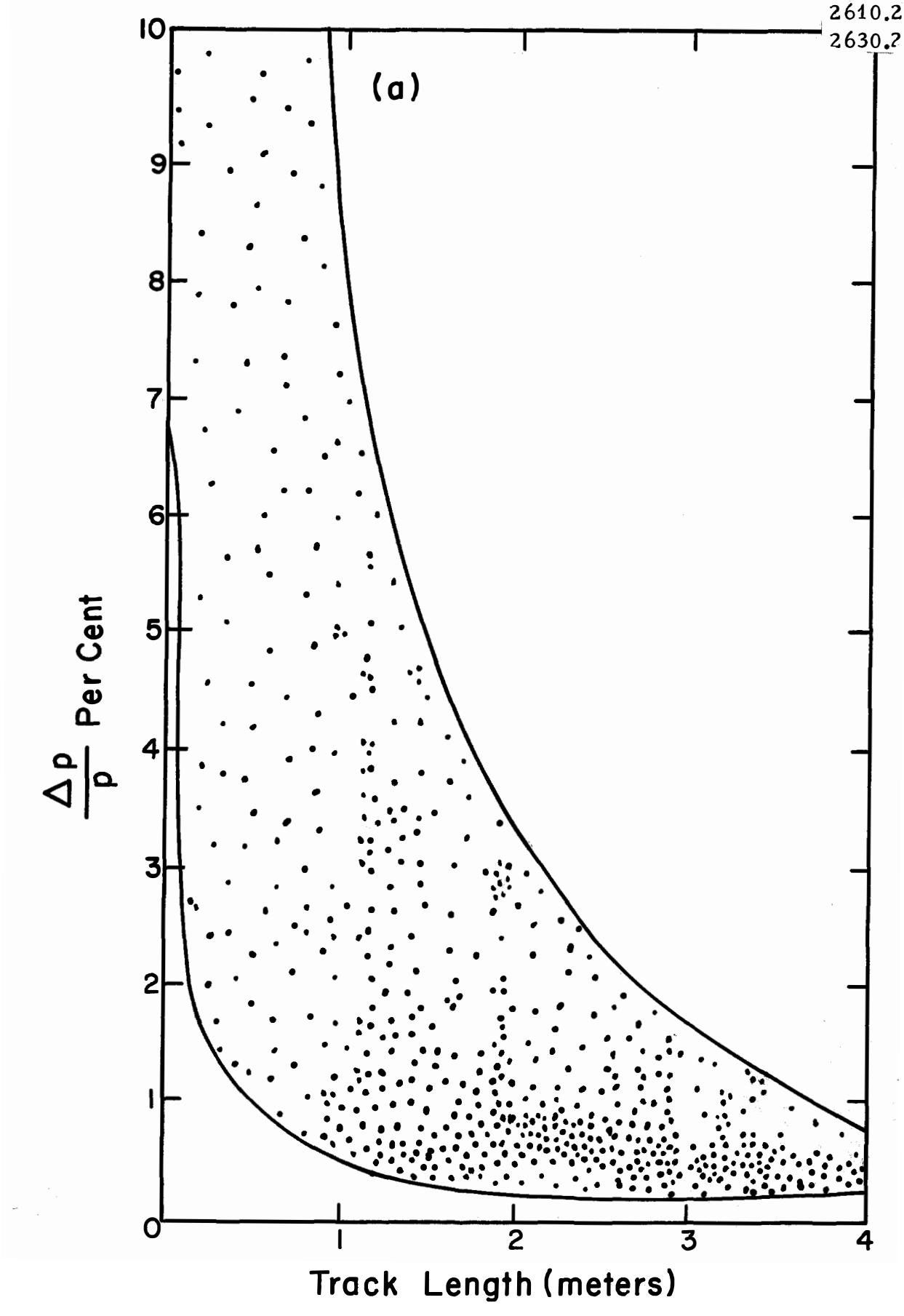

Fig. 13a. Same as Fig. 12a, with annihilation at 100 Gev/c.

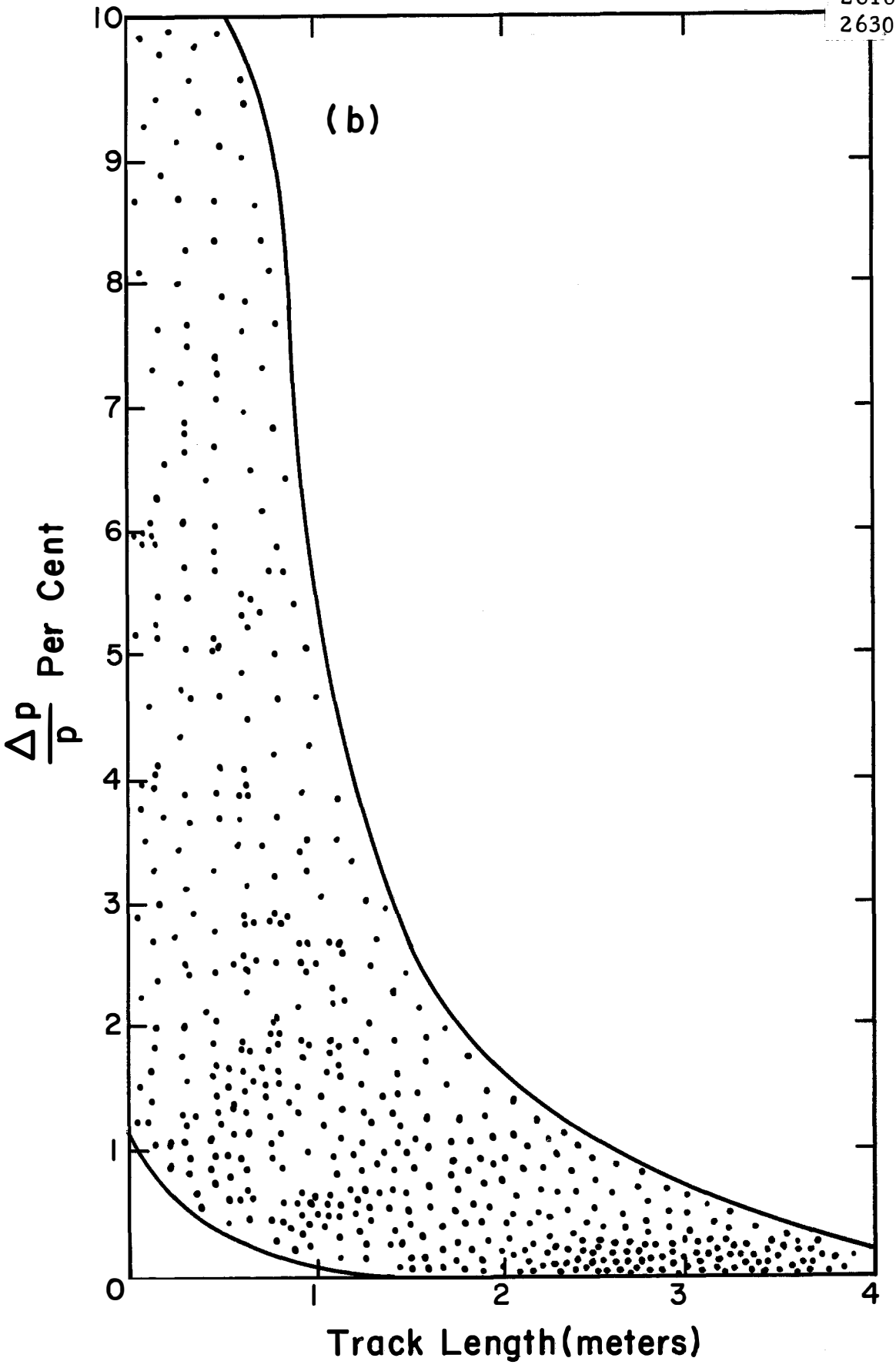

Fig. 13b. Same as 12b, reaction at 100 Gev/c.

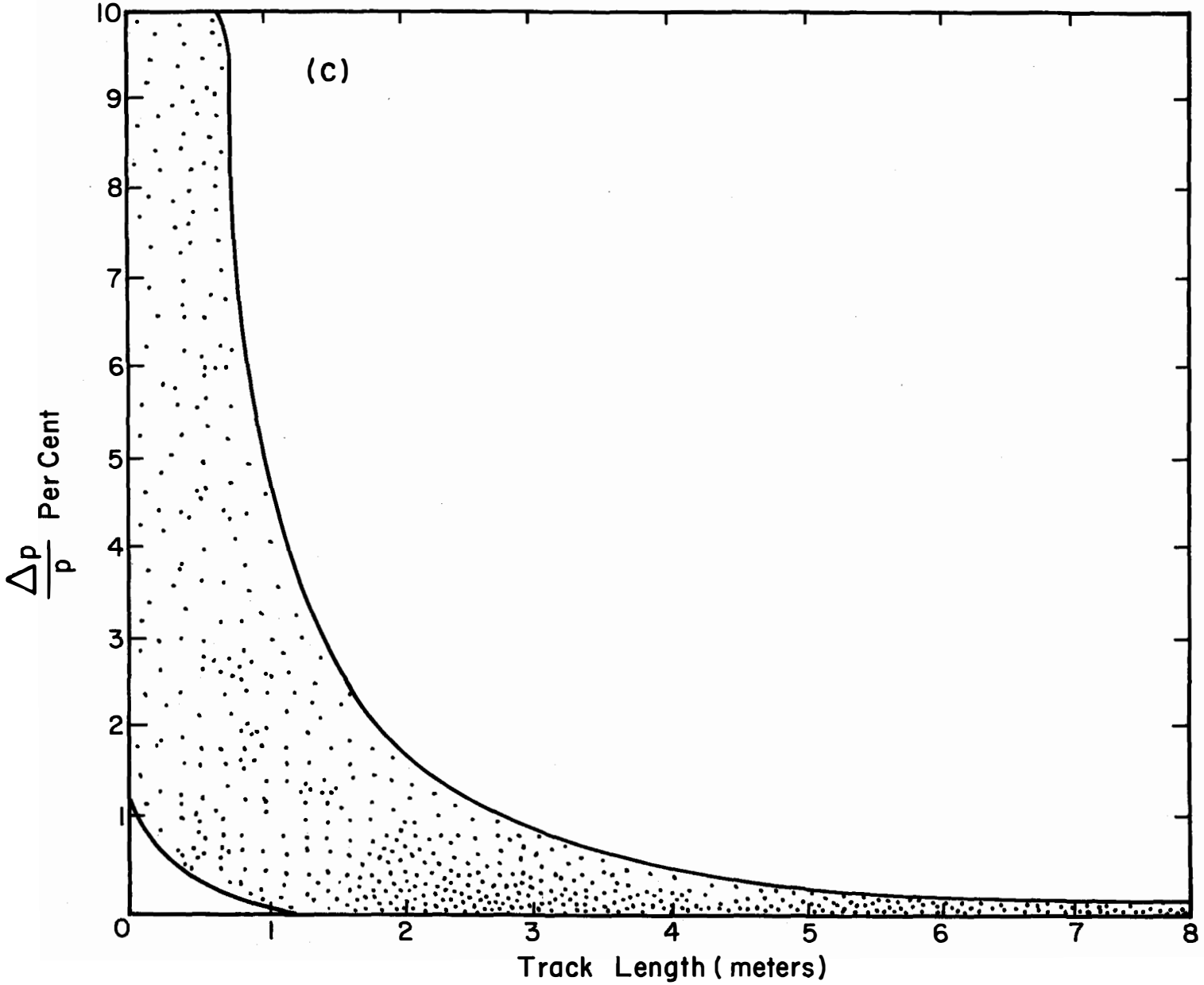

Fig. 13c. Same as 12c, reaction at 100 Gev/c.

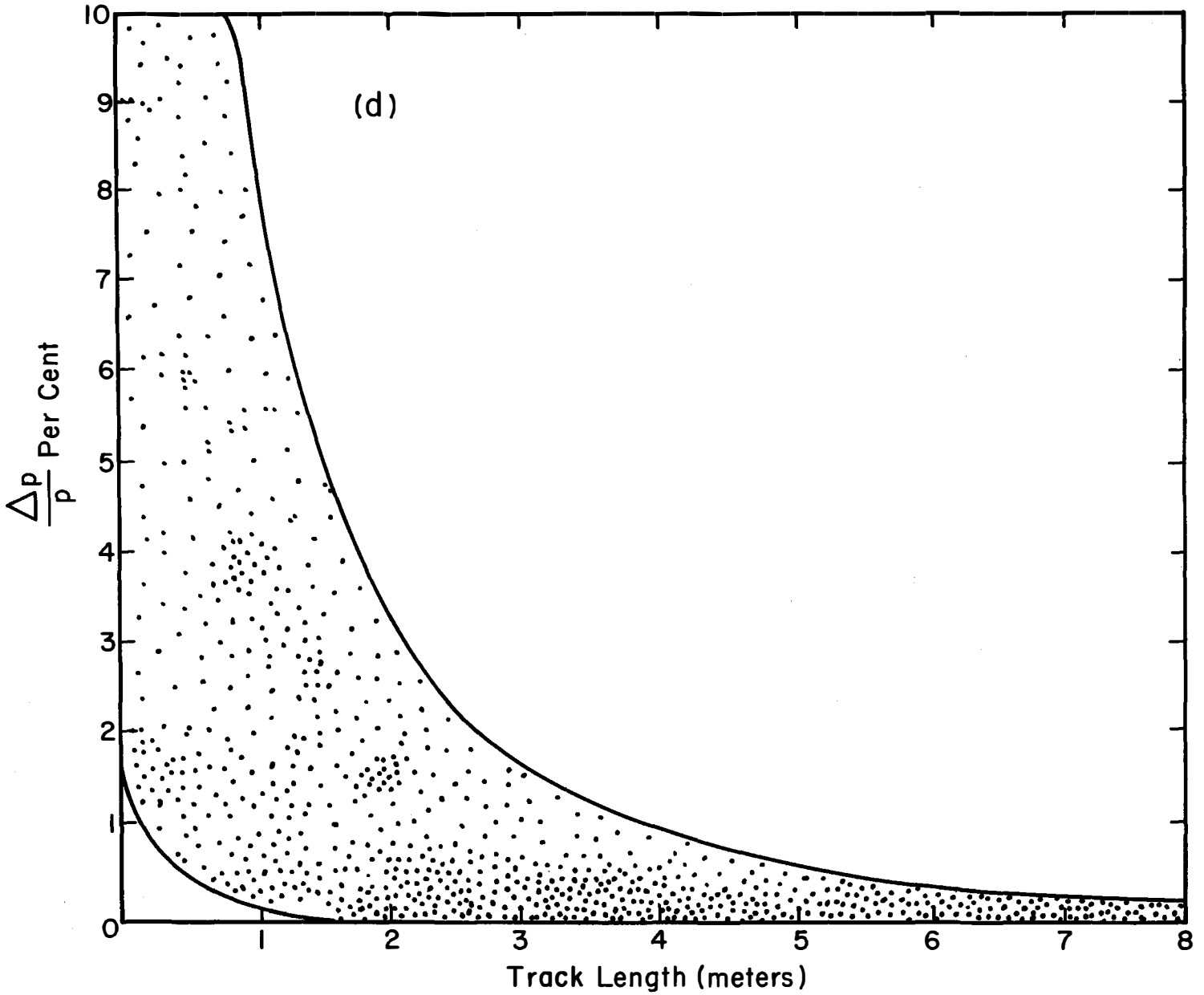

Fig. 13d. Same as 12d, reaction at 100 Gev/c.

TM-151
2610.2
2630.2

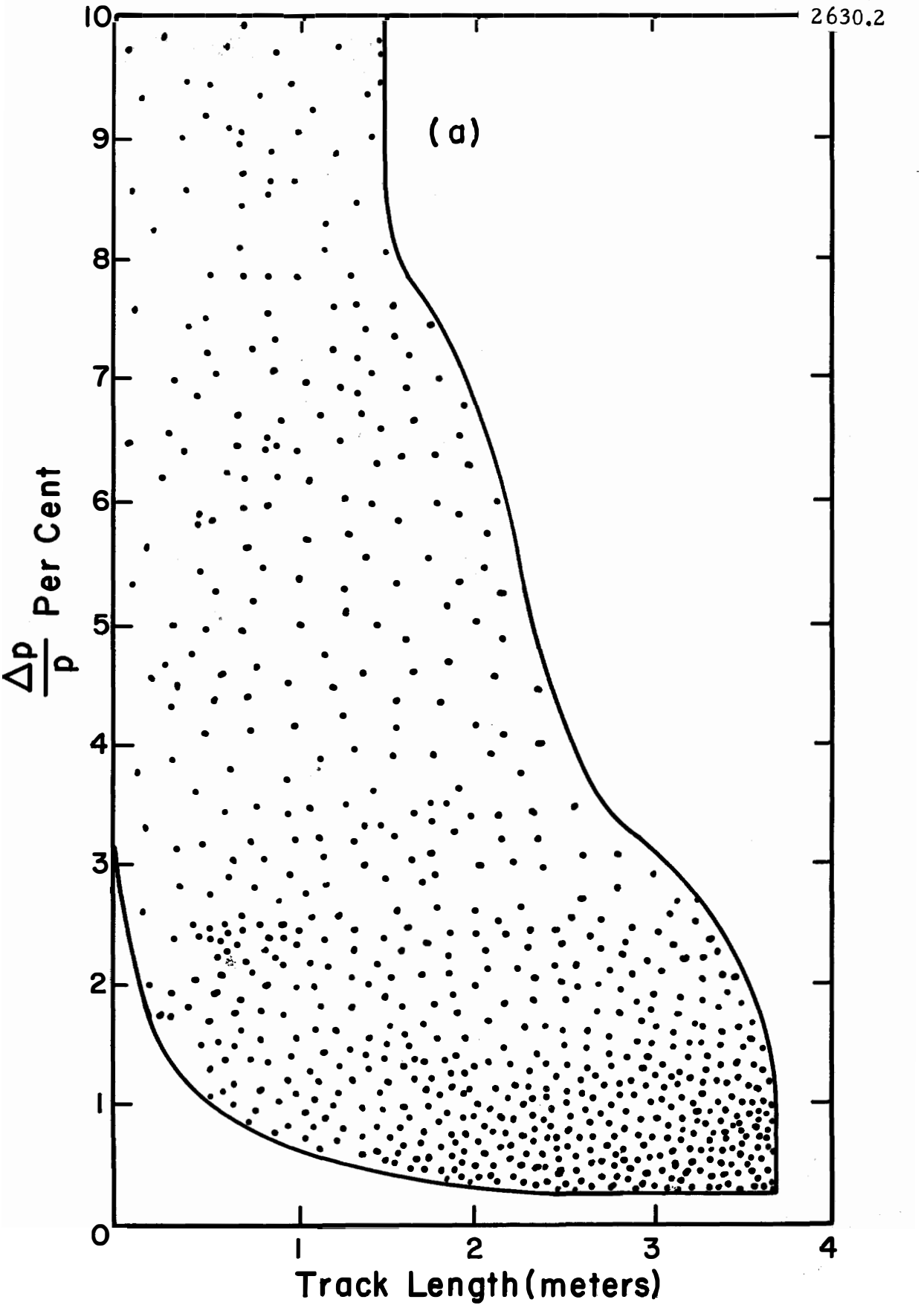

Fig. 14a. Same as Fig. 12a, with reaction at 200 Gev/c.

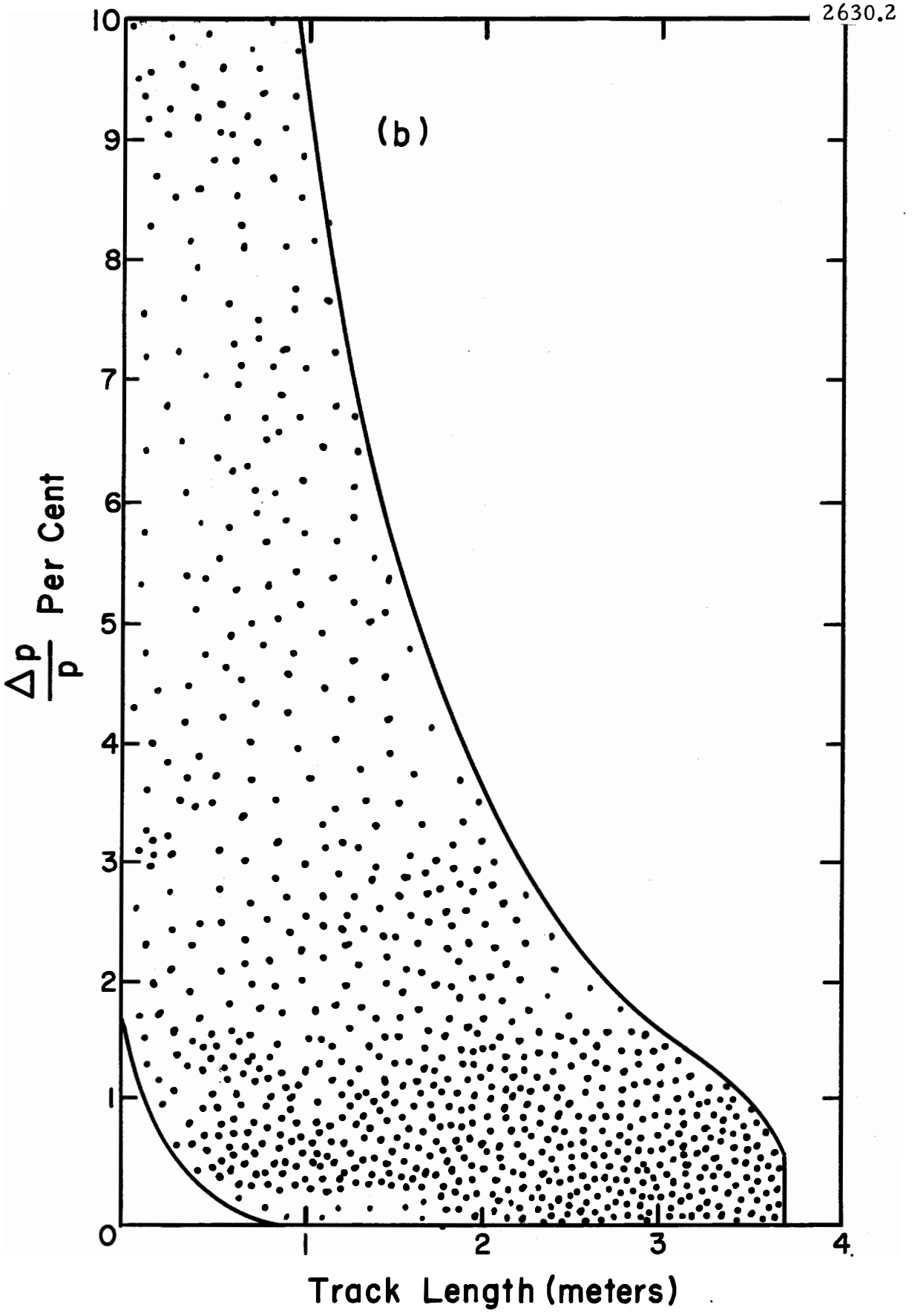

Fig. 14b. Same as 12b, reaction at 200 Gev/c.

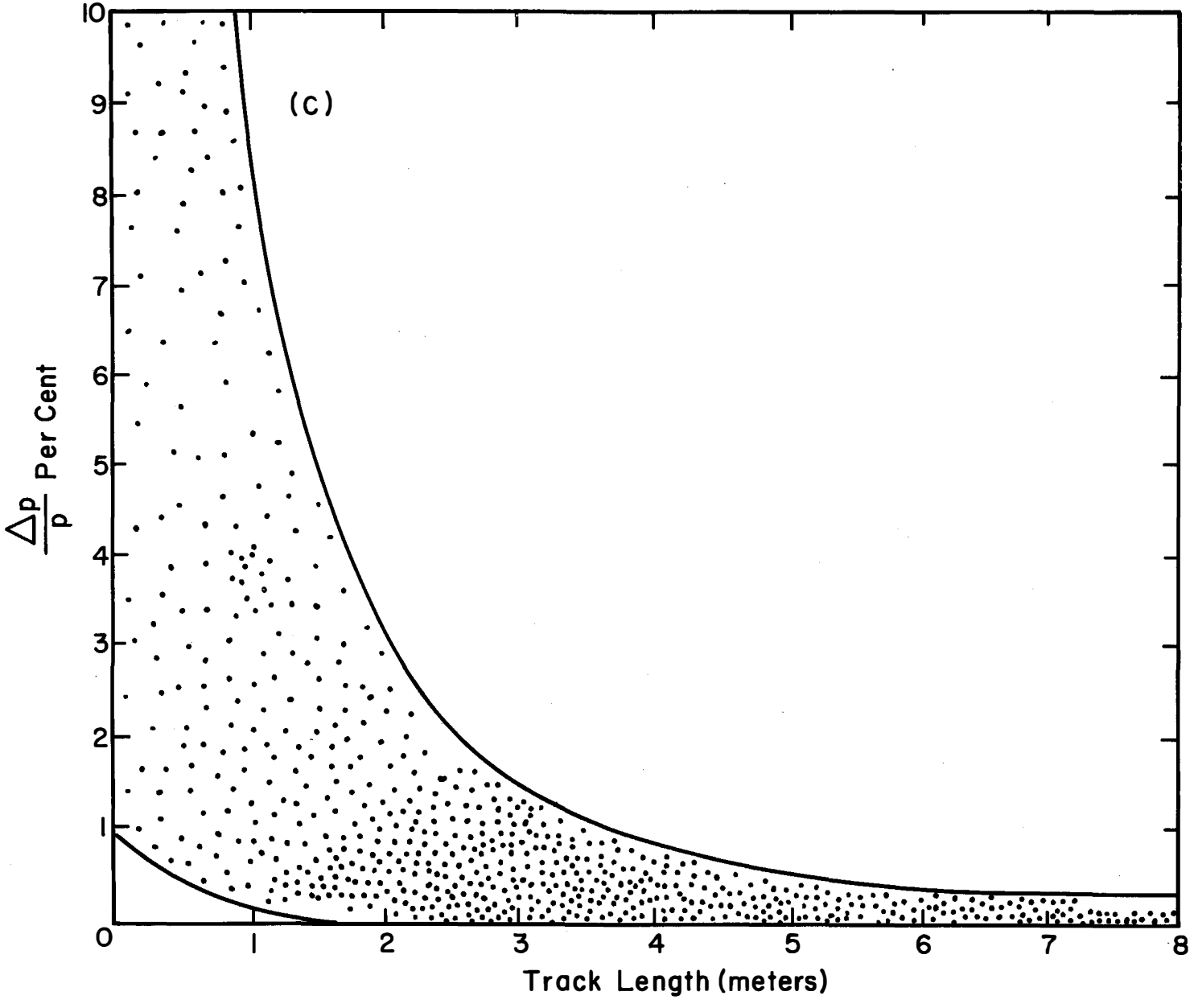

Fig. 14c. Same as 12c, reaction at 200 Gev/c.

TM-151
2610.2
2630.2

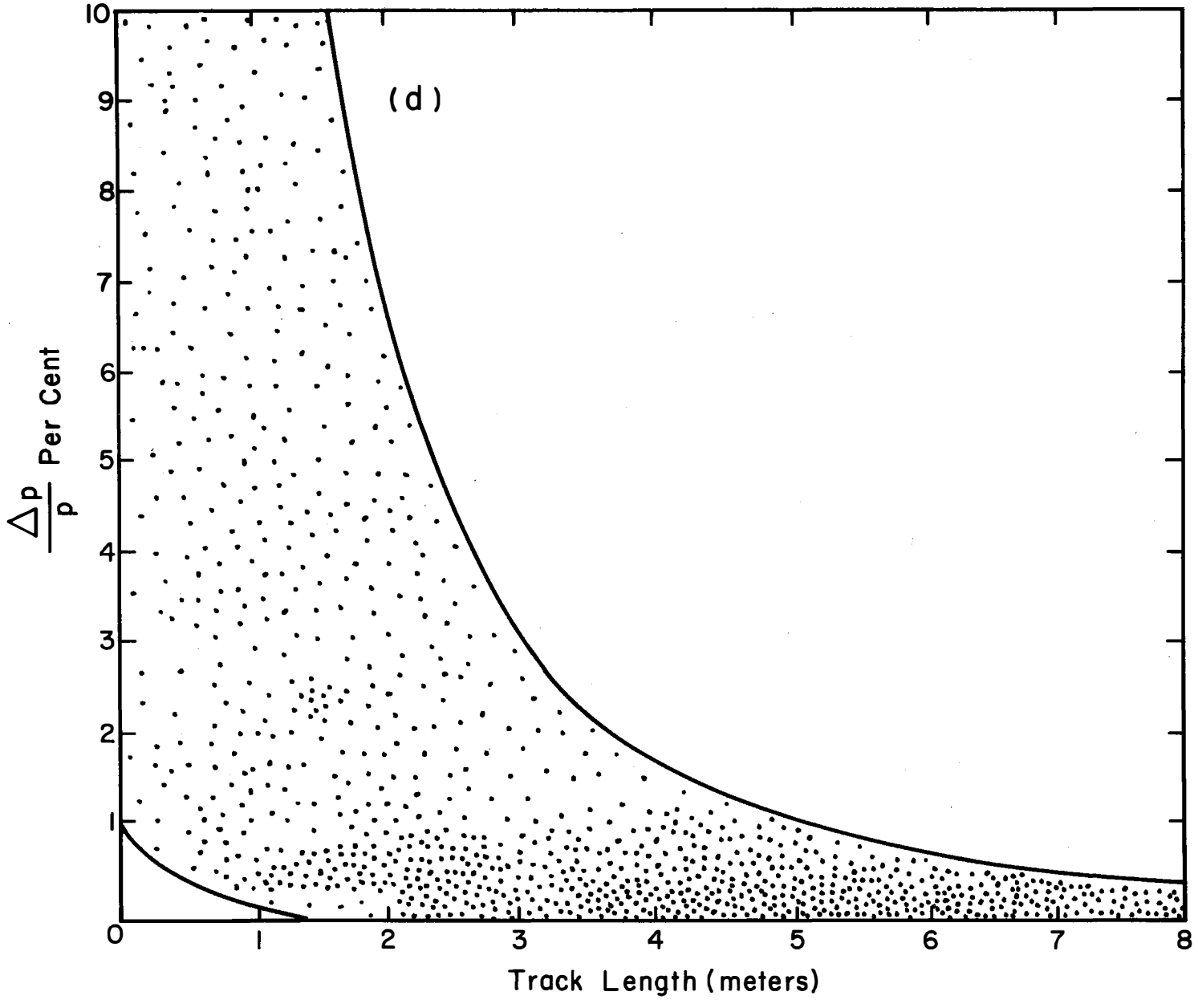

Fig. 14d. Same as 12d, reaction at 200 Gev/c.

TM-151
2610.2
2630.2

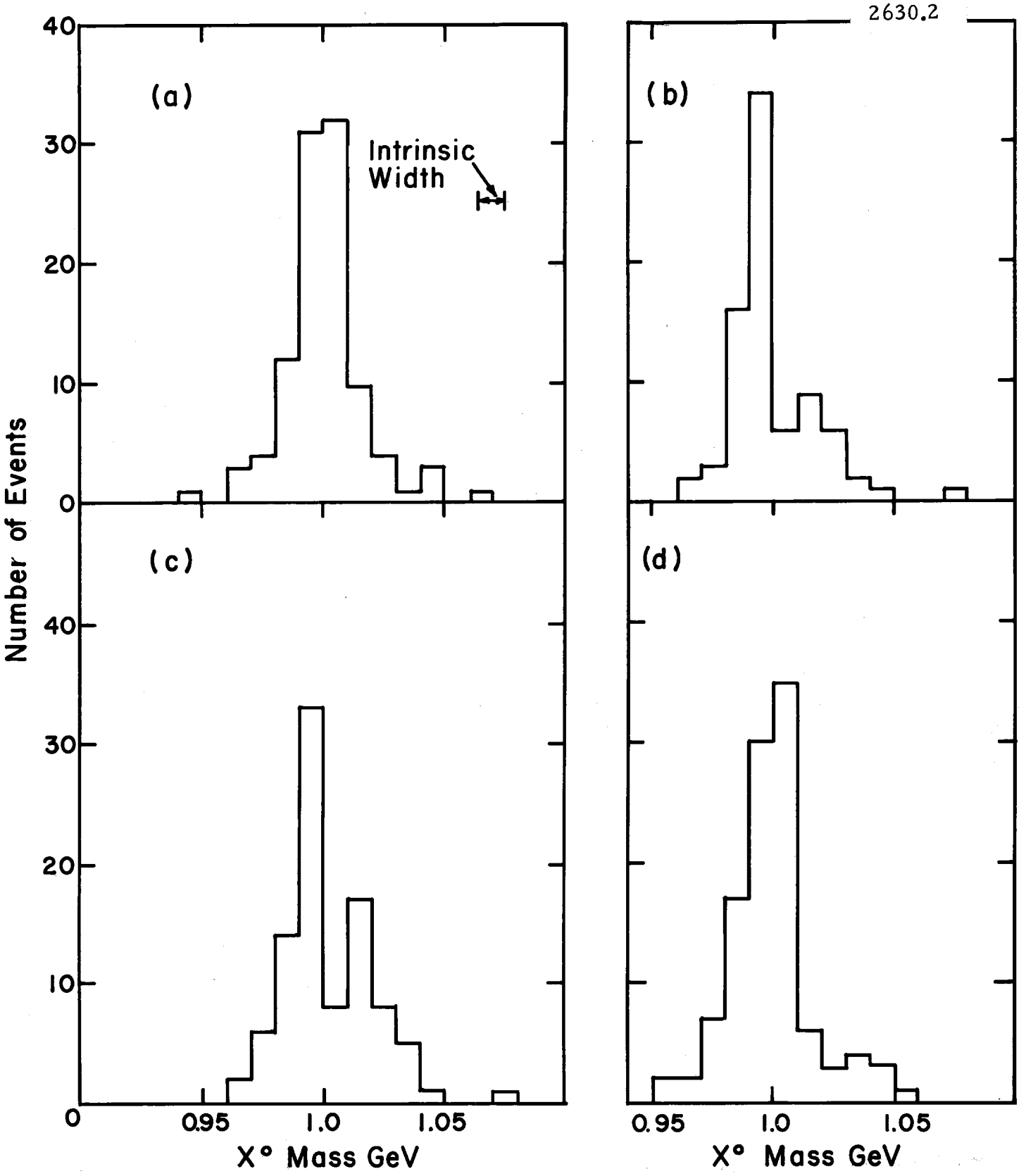

Fig. 15. Mass Resolution for missing mass X^o observed in the reaction $\bar{p} + p \rightarrow 2\pi^+ 2\pi^- X^o$, with subsequent decay $X^o \rightarrow \pi^+ \pi^-$, at 50 Gev/c. 15a-d, bubble chamber operating conditions as in previous curves, e.g. Fig. 4.

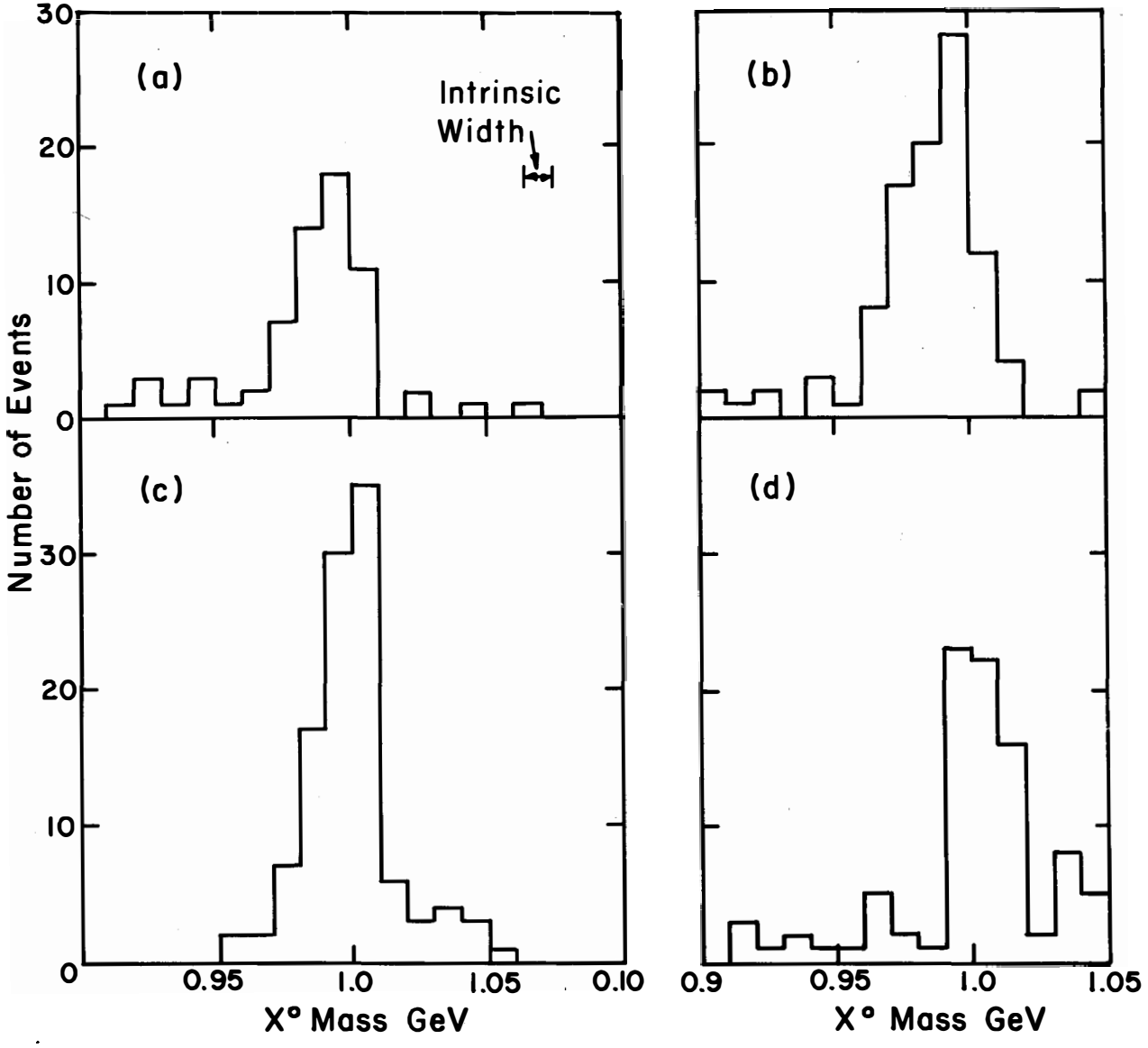

Fig. 16. Same as Fig. 15, except at 200 Gev/c.

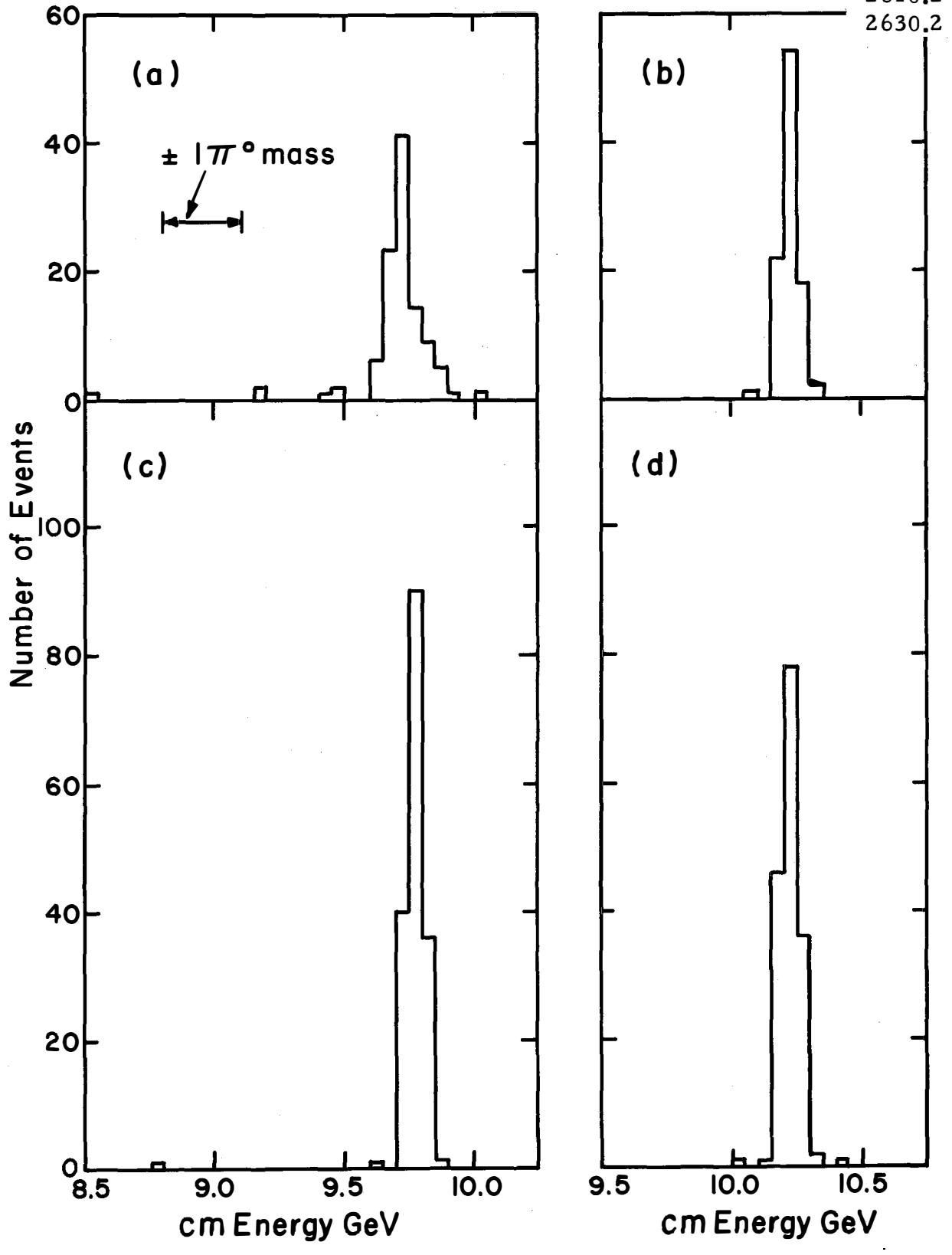

Fig. 17. Resolution of cm energy, same reaction as Fig. 9, at 50 Gev/c.

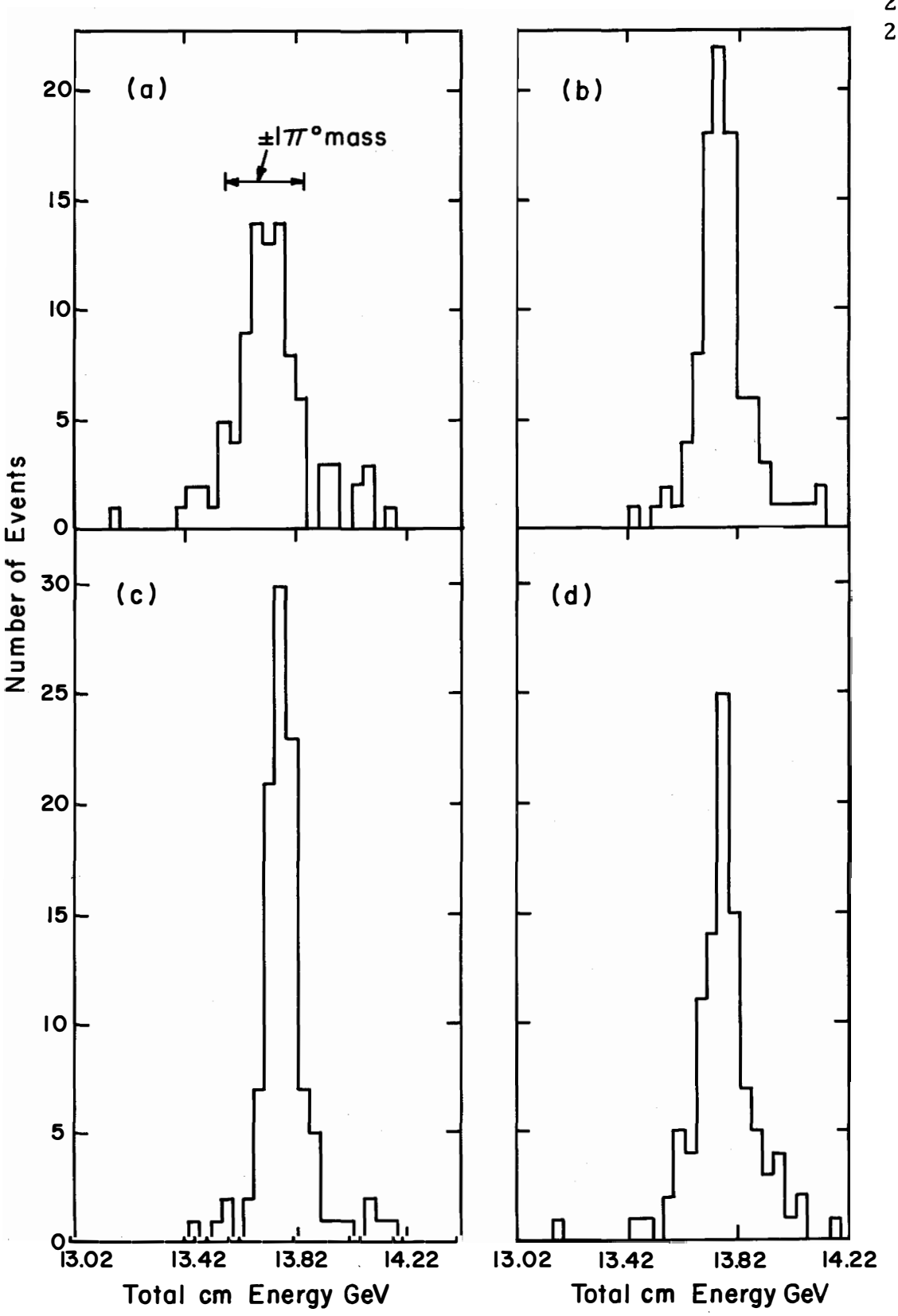

Fig. 18. Same as Fig. 17, at 100 Gev/c.

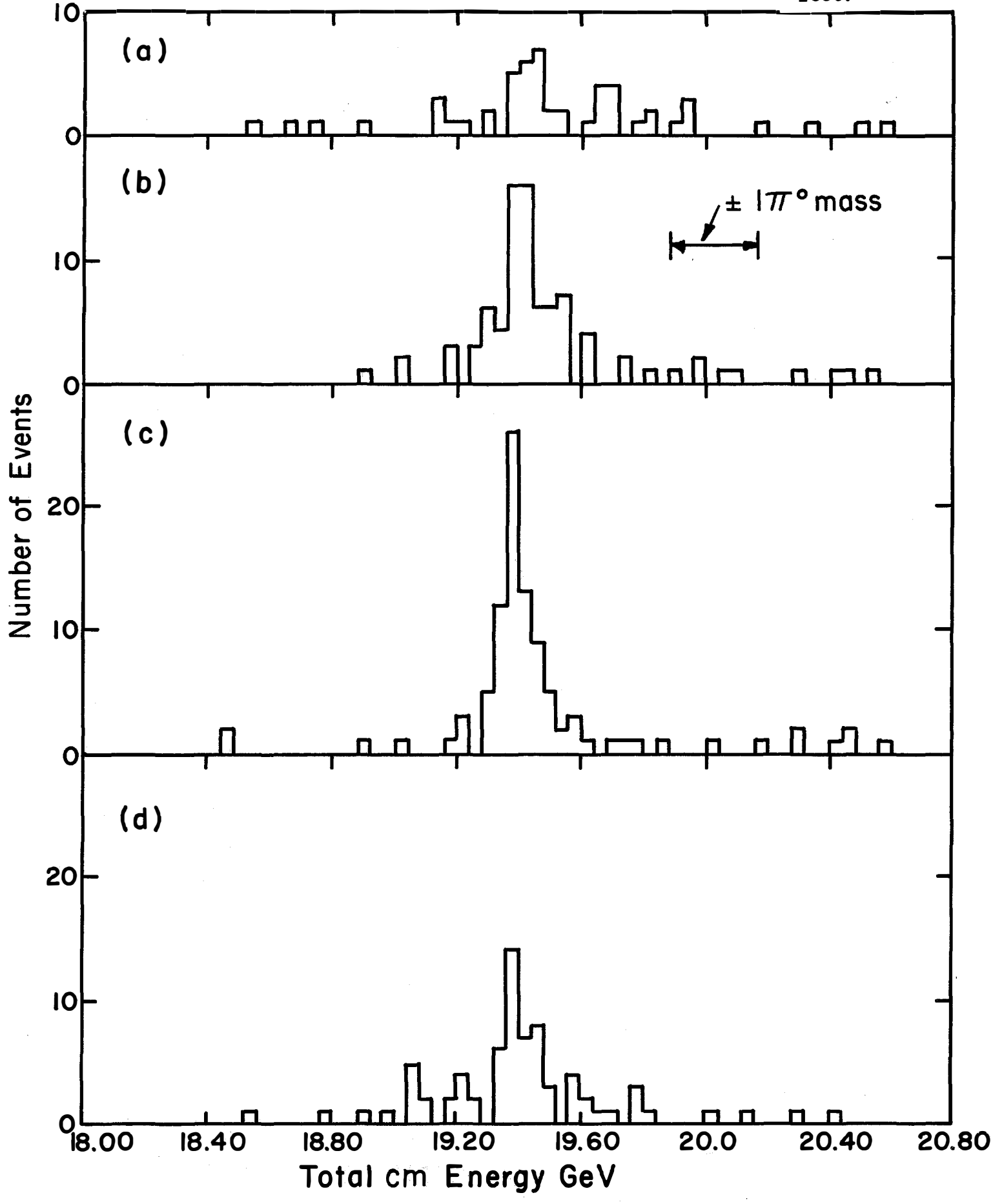

Fig. 19. Same as Fig. 17, at 200 Gev/c.

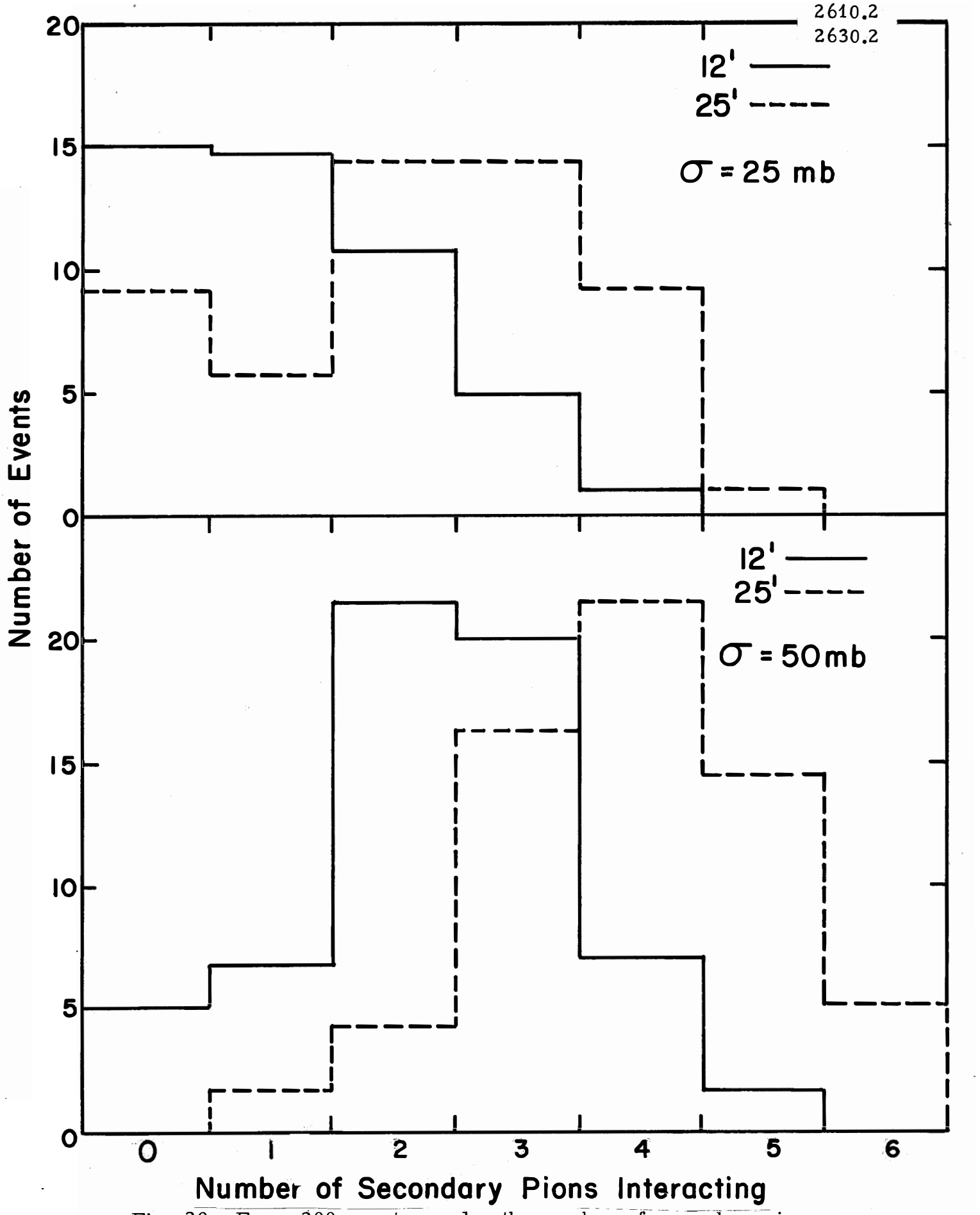

Fig. 20. For a 200-event sample, the number of secondary pions interacting, produced in upstream events in the reaction $\bar{p} + p \rightarrow 3\pi^+ 3\pi^-$. For case b, $\sigma = 60$ mb; note the absence of any events in the 25-ft chamber with the secondary pions interacting.